



HAL
open science

Convective dissolution of Carbon Dioxide in two- and three-dimensional porous media: the impact of hydrodynamic dispersion

Jayabrata Dhar, Patrice Meunier, F. Nadal, Yves Méheust

► **To cite this version:**

Jayabrata Dhar, Patrice Meunier, F. Nadal, Yves Méheust. Convective dissolution of Carbon Dioxide in two- and three-dimensional porous media: the impact of hydrodynamic dispersion. *Physics of Fluids*, 2022, 34 (6), pp.064114. 10.1063/5.0086370 . insu-03702425

HAL Id: insu-03702425

<https://insu.hal.science/insu-03702425>

Submitted on 23 Jun 2022

HAL is a multi-disciplinary open access archive for the deposit and dissemination of scientific research documents, whether they are published or not. The documents may come from teaching and research institutions in France or abroad, or from public or private research centers.

L'archive ouverte pluridisciplinaire **HAL**, est destinée au dépôt et à la diffusion de documents scientifiques de niveau recherche, publiés ou non, émanant des établissements d'enseignement et de recherche français ou étrangers, des laboratoires publics ou privés.

This is the author's peer reviewed, accepted manuscript. However, the online version of record will be different from this version once it has been copyedited and typeset.

PLEASE CITE THIS ARTICLE AS DOI: 10.1063/5.0086370

Accepted to Phys. Fluids 10.1063/5.0086370

Convective dissolution of Carbon Dioxide in porous media: impact of dispersion AIP/123-QED

Convective dissolution of Carbon Dioxide in two- and three-dimensional porous media: the impact of hydrodynamic dispersion

J. Dhar,¹ P. Meunier,² F. Nadal,³ and Y. Méheust¹

¹*Univ. Rennes, CNRS, Géosciences Rennes (UMR6118), 35042 Rennes, France*

²*Aix Marseille Université, Centrale Marseille, CNRS, IRPHE, 13384 Marseille, France*

³*Wolfson school of Mechanical and Electrical Engineering, Loughborough University, Loughborough, UK*

(*Electronic mail: yves.meheust@univ-rennes1.fr)

(Dated: 4 May 2022)

This is the author's peer reviewed, accepted manuscript. However, the online version of record will be different from this version once it has been copyedited and typeset.

PLEASE CITE THIS ARTICLE AS DOI: 10.1063/5.0086370

Accepted to *Phys. Fluids* 10.1063/5.0086370

Convective dissolution of Carbon Dioxide in porous media: impact of dispersion

Convective dissolution is the process by which CO_2 injected in geological formations dissolves into the aqueous phase and thus remains stored perennially by gravity. It can be modeled by buoyancy-coupled Darcy flow and solute transport. The transport equation should include a diffusive term accounting for hydrodynamic dispersion, wherein the effective diffusion coefficient is proportional to the local interstitial velocity. We investigate the impact of the hydrodynamic dispersion tensor on convective dissolution in two-dimensional (2D) and three-dimensional (3D) homogeneous porous media. Using a novel numerical model we systematically analyze, among other observables, the time evolution of the fingers' structure, dissolution flux in the quasi-constant flux regime, and mean concentration of the dissolved CO_2 ; we also determine the onset time of convection, t_{on} . For a given Rayleigh number Ra , the efficiency of convective dissolution over long times is controlled by t_{on} . For porous media with a dispersion anisotropy commonly found in the subsurface, t_{on} increases as a function of the longitudinal dispersion's strength (S), in agreement with previous experimental findings and in contrast to previous numerical findings, a discrepancy which we explain. More generally, for a given strength of transverse dispersion, longitudinal dispersion always slows down convective dissolution, while for a given strength of longitudinal dispersion, transverse dispersion always accelerates it. Furthermore, systematic comparison between 2D and 3D results shows that they are consistent on all accounts, except for a slight difference in t_{on} and a significant impact of Ra on the dependence of the finger number density on S in 3D.

Convective dissolution of Carbon Dioxide in porous media: impact of dispersion

I. INTRODUCTION

It is now widely admitted that the global warming of the Earth's atmosphere observed since the beginning of the industrial era, in particular in the last 30 years, mostly results from an increase in the concentration of atmospheric greenhouse gases, among which CO_2 is responsible for about two-thirds of the temperature increase¹. In this context, the storage of CO_2 in deep geological formations (deep saline aquifers and depleted oil/gas reservoirs) is widely regarded as the most promising measure to limit global warming, and has thus attracted much attention from the scientific and engineering communities. Upon injection at depths larger than 900 m, CO_2 is in its supercritical state (scCO_2), where it is less dense than the resident brine, so that it rises towards the top of the geological formation where it is trapped under an impermeable cap rock. At the scCO_2 -brine interface, scCO_2 partially dissolves into the brine, thereby forming an aqueous layer of brine enriched with dissolved CO_2 , that is denser than the brine located underneath. Hence this unstable stratification of the two miscible fluids (scCO_2 and brine) leads to a gravitational instability wherein the ensuing convection allows the dissolved scCO_2 to be transported deeper into the formation, while fresh CO_2 -devoid brine is brought to the scCO_2 -brine interface, allowing CO_2 to further dissolve into the aqueous phase²⁻⁴. This so-called dissolution trapping mechanism allows for perennial trapping of CO_2 by gravity within the resident brine. The total storage capacity is constrained by the available porous volume and dissolution of scCO_2 into the brine.

But the flow dynamics at play until that capacity is reached is complex. It initiates with the formation of a transient diffusive layer of brine- CO_2 mixture that strongly damps small perturbations until a critical time is reached. After that time, the gravitational instability develops, first in the linear regime where the growth of perturbations to the miscible interface is exponential^{5,6}. In this regime the total diffusive flux at the top boundary of the flow domain (also equal to the total dissolution flux as no convective flux exists on that boundary) decreases while the convective perturbations grow. The strength of the convection (with respect to molecular diffusion) is quantified by the non-dimensional Rayleigh number. The time at which the total dissolution flux starts increasing again, called the nonlinear onset time, is that at which the convective process can be considered to develop. The total flux then reaches a (quasi-)constant flux regime in which it fluctuates around a plateau value which is all the better defined as the Rayleigh number is larger⁷. The so-called shutdown regime that follows results from the progressive rise in the mean solute CO_2 concentration in the brine, which weakens the convection.

Convective dissolution of Carbon Dioxide in porous media: impact of dispersion

Understanding this dynamics is crucial for the prediction of the characteristic time scale of dissolution trapping in particular, and of the subsurface sequestration of CO₂ in general. Hence convective dissolution has been the topic of many past studies, either based on experiments in Hele-Shaw cells (i.e., setups analog to a homogeneous two-dimensional – 2D – porous medium, see Vreme *et al.*⁸) or in granular porous media imaged using optical methods^{9,10} or X-ray tomography^{11,12,13}, or on theoretical/numerical simulations^{6,14–16}, to name a few. Among the latter, only a handful^{17–20} have presented three-dimensional (3D) simulations (which are somewhat more common in thermal convection studies²¹).

Not considering potential chemical reactions between the dissolved CO₂ and either the solid phase (the so-called mineral trapping) or other solutes, Darcy-scale theoretical modeling of convective dissolution describes the buoyancy-driven hydrodynamics and transport of dissolved CO₂, coupled through the dependence of the brine's density on the local concentration in dissolved CO₂. At the Darcy scale, solute diffusion does not only result from molecular diffusion, but also from hydrodynamic (or, mechanical) dispersion, which is the Darcy-scale manifestation of the pore scale interaction between molecular diffusion and heterogeneous advection²². A well-posed formulation of the transport equation should thus include a diffusive term accounting for hydrodynamic dispersion, i.e., involving a dispersion tensor that is proportional to the magnitude of the local velocity vector as well as anisotropic, since mechanical dispersion is typically one order of magnitude larger along the local velocity's direction than along the transverse direction^{23,24}; the dispersivity lengths which define the linear transformation to be applied to the local velocity are intrinsic properties of the porous medium. Such a dispersive term can potentially turn the dynamics highly non-linear.

In effect, many of the aforementioned numerical studies (either 2D or 3D) have considered simple diffusive transport, either because considering only molecular diffusion allows for analytical developments otherwise intractable, or because they considered a Péclet number sufficiently small for the impact of dispersion to always be negligible with respect to that of molecular diffusion (this hypothesis being in any case reasonable at the initiation of the instability). In particular, to our knowledge, those among the 3D numerical studies which have accounted for hydrodynamic dispersion have not investigated its effect in detail, but have rather focused on the effect of carbonate geochemical reactions²⁵. Furthermore, while the nonlinear onset time is known from numerical and experimental studies alike to decrease with the Rayleigh number^{2,4,5,12}, the literature has reported conflicting views regarding the influence of hydrodynamic dispersion on the onset of

Convective dissolution of Carbon Dioxide in porous media: impact of dispersion

gravitational instability^{26,27}. Numerical studies^{14,28} have predicted that the nonlinear onset time decreases monotonically with the strength of hydrodynamic dispersion, and that this reduction may reach two orders of magnitude. On the contrary, the theoretical/numerical by Emami-Meybodi²⁹ reported an increase of the nonlinear onset time when the dispersion strength is increased, in the presence of a horizontal background flow, and experimental studies^{9,30} have reported an evolution of the convection's structure when increasing the dispersion strength that also indicates a weakening of convection. Moreover, the impact of the dispersion tensor's anisotropy has been little studied systematically; the numerical predictions of Refs.^{28,31} indicate that its overall effect on the efficiency of convective dissolution is negligible.

In this study, we use an in-house numerical model accounting for anisotropic hydrodynamic dispersion and implemented using the open-source computational fluid dynamics (CFD) platform OpenFOAM to investigate convective dissolution in 2D and 3D geometries. Our objectives are two-fold. Firstly, to investigate systematically how the strength of hydrodynamic dispersion (relative to molecular diffusion), and the anisotropy of its tensor impact convective dissolution. In doing so we explain the discrepancy between the conclusions drawn in previous numerical and experimental studies on the impact of hydrodynamic dispersion on the nonlinear onset time; our own numerical results are consistent with the experimental observations. Secondly, to compare systematically the results obtained in the 2D and 3D geometries, all parameters being equal otherwise, to assess the role of space dimensionality on model predictions. The numerical model is based on a stream function formulation. The parameter space is investigated as widely as possible given the large computational times associated in particular to 3D numerical simulation: three dispersion strengths, three to four dispersivity length anisotropies, two Rayleigh numbers. The assessment of the impact of hydrodynamic dispersion is based on all available physical observables: the solute fingers' number density (FND), penetration depth and maximum velocity; the nonlinear onset time of convection; the dissolution flux in the quasi-constant flux regime; the mean concentration of the dissolved CO₂; and the scalar dissipation rate.

The theoretical model and its numerical implementation are described in section II. The systematic investigation of the dependence of all aforementioned observables on the dispersion strength and dispersivity length anisotropy is presented in section III. In the Discussion (section IV) we provide a synthesis of our findings on the role of dispersion, and confront these results to those of previous studies on the topic; we also discuss the role of space dimensionality. Finally the Conclusion presents a short summary of the content of the paper, a synthesis of its main

Convective dissolution of Carbon Dioxide in porous media: impact of dispersion

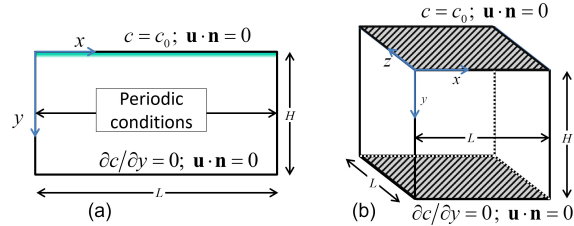


FIG. 1. Schematics of the two-dimensional (a) and three-dimensional (b) configurations and boundary conditions; the boundary conditions associated to the governing equations (2) are indicated.

finding, and some prospects for future studies.

II. MODEL OF CONVECTIVE DISSOLUTION IN A HOMOGENEOUS POROUS MEDIUM

A. Theoretical Formulation and boundary conditions

We consider a porous medium described at the Darcy (i.e., continuum) scale as homogeneous and isotropic, i.e. with uniform porosity ϕ , scalar permeability κ , and dispersivity lengths α_L and α_T , where the notations L and T refer respectively to the longitudinal and transverse direction with respect to the local velocity vector. The flow domain is assumed to be a rectangle (in two dimensions – 2D) or a rectangle cuboid (in three dimensions – 3D) of height H in the vertical (y) direction and length L in the horizontal direction(s) (x in 2D, x and z in 3D), see Fig. 1.

This domain is initially filled with pure brine. At the top boundary of the domain the brine is in contact with supercritical CO_2 (sCO_2 , outside of the flow domain of Fig. 1) which partially dissolves into the brine, rendering the density of the brine- CO_2 mixture dependent on the local concentration c of the dissolved CO_2 according to a linear dependence $\rho = \rho_0 + (c/c_0)\Delta\rho$, where ρ_0 , c_0 and $\Delta\rho$ denote respectively the density of pure brine, the saturation concentration of the dissolved CO_2 , which is controlled by its solubility in the brine, and the density difference between the mixture at concentration c_0 and the pure brine.

The dissolution of supercritical CO_2 into brine is usually a much quicker process than the onset of instability, so its impact on the concentration of the dissolved CO_2 at the brine- sCO_2 interface ($y = 0$ plane) can be safely assumed to result in a constant boundary concentration c_0

Convective dissolution of Carbon Dioxide in porous media: impact of dispersion

on that plane. The bottom boundary of the domain ($y = H$ plane) is assumed impermeable while periodic boundary conditions are imposed on all lateral boundaries. With this picture in mind, the boundary condition for the concentration c and the velocity field \mathbf{u} of the solution are as follows:

$$\begin{aligned} \mathbf{u}(x, 0, [z, t]) \cdot \hat{\mathbf{y}} &= 0; & c(x, 0, [z, t]) &= c_0 \\ \mathbf{u}(x, H, [z, t]) \cdot \hat{\mathbf{y}} &= 0; & \frac{\partial c}{\partial y}(x, H, [z, t]) &= 0 \\ \mathbf{u}(0, y, [z, t]) &= \mathbf{u}(L, y, [z, t]); & c(0, y, [z, t]) &= c(L, y, [z, t]) \\ [\mathbf{u}(x, y, 0, t) &= \mathbf{u}(x, y, L, t); & c(x, y, 0, t) &= c(x, y, L, t)] \end{aligned} \quad (1)$$

where t is time, $\hat{\mathbf{y}}$ is the unit vector along axis y , and the brackets $[\dots]$ indicate equations or terms that are only present for the 3D geometry. Note that we have assumed that the interface between the supercritical CO_2 and the aqueous phase remains at all times horizontal and positioned at the top boundary of the flow domain.

The classical Boussinesq approximation being applied on account of the small CO_2 solubility, the mass conservation and coupled flow and solute transport in the porous medium are described respectively by the following governing equations:

$$\nabla \cdot \mathbf{u} = 0 \quad (2a)$$

$$\mathbf{u} = -\frac{\kappa}{\eta} (\nabla p - \rho g \hat{\mathbf{y}}) \quad \text{with} \quad \rho = \rho_0 + \Delta\rho \frac{c}{c_0} \quad (2b)$$

$$\phi \frac{\partial c}{\partial t} + \mathbf{u} \cdot \nabla c = \phi \nabla \cdot (\bar{\mathbf{D}} \cdot \nabla c) \quad (2c)$$

where p is the pressure field and η the fluid's viscosity (assumed independent of c), while $\bar{\mathbf{D}}$ denotes the dispersion tensor. This tensor incorporates molecular diffusion but is also dependent on the local velocity through a non-diagonal component that accounts for hydrodynamic dispersion and is, in general, anisotropic even for an isotropic porous medium. Therefore, in a reference frame locally attached to the streamline, $\bar{\mathbf{D}}$ takes the form $\bar{\mathbf{D}} = D_0 \bar{\mathbf{I}} + \bar{\mathbf{D}}_{\text{disp}}$, where D_0 is the molecular diffusion coefficient, $\bar{\mathbf{I}}$ is the identity matrix and the *hydrodynamic* (or *mechanical*) dispersion tensor $\bar{\mathbf{D}}_{\text{disp}}$ has the form

$$\bar{\mathbf{D}}_{\text{disp}} = \frac{1}{\phi} \begin{bmatrix} \alpha_L \|\mathbf{u}\| & 0 \\ 0 & \alpha_T \|\mathbf{u}\| \end{bmatrix}. \quad (3)$$

After transforming the dispersion tensor $\bar{\mathbf{D}}$ back into the (x, y, z) cartesian reference frame, it takes the well-known form¹⁴

$$D_{ij} = D_0 \delta_{ij} + D_{ij}^{\text{disp}} \quad \text{with} \quad D_{ij}^{\text{disp}} = \frac{\alpha_T}{\phi} \|\mathbf{u}\| \delta_{ij} + \frac{\alpha_L - \alpha_T}{\phi} \frac{u_i u_j}{\|\mathbf{u}\|}, \quad (4)$$

Convective dissolution of Carbon Dioxide in porous media: impact of dispersion

where δ_{ij} is the Kronecker delta function and $\|\mathbf{u}\|$ the Euclidean norm of the velocity.

B. Non-dimensionalisation of governing equations

We proceed to non-dimensionalize the above formulation by considering the following scales for length, velocity, time, pressure and concentration, respectively: H , $u^* = \kappa\Delta\rho g/\eta$, $t^* = \phi H/u^*$, $\Delta\rho gH$ and c_0 . The dimensionless form of the governing equations thus reads

$$\tilde{\nabla} \cdot \tilde{\mathbf{u}} = 0 \quad (5a)$$

$$\tilde{\mathbf{u}} = -(\tilde{\nabla} \tilde{p} - \tilde{c} \hat{\mathbf{y}}) \quad (5b)$$

$$\frac{\partial \tilde{c}}{\partial \tilde{t}} + \tilde{\mathbf{u}} \cdot \tilde{\nabla} \tilde{c} = \frac{1}{Ra} \tilde{\nabla} \cdot (\tilde{\mathbf{D}} \cdot \tilde{\nabla} \tilde{c}), \quad (5c)$$

where the $\tilde{}$ sign denotes a non-dimensional quantity,

$$Ra = \frac{\Delta\rho g \kappa H}{\phi \eta D_0} \quad (6)$$

is the Rayleigh number, and the dimensionless form of the dispersion tensor recasts as

$$\tilde{\mathbf{D}} = (1 + S\alpha\|\tilde{\mathbf{u}}\|)\mathbf{I} + S(1 - \alpha) \frac{\tilde{u}_i \tilde{u}_j}{\|\tilde{\mathbf{u}}\|}. \quad (7)$$

Here

$$S = \frac{\alpha_L u_{\text{ref}}}{D_0 \phi} \quad \text{and} \quad \alpha = \frac{\alpha_T}{\alpha_L} \quad (8)$$

are respectively the longitudinal dispersion's strength as compared to molecular diffusion and the dispersivity ratio, which is a measure of the medium's dispersive anisotropy. Note that the reference time t^* and Rayleigh number are independent of the dispersion properties, namely, longitudinal dispersion strength and dispersivity ratio. This is appropriate as the dispersivity lengths are a property of the geometrical structure of the porous medium while molecular diffusion is typically independent of the medium's structure for the range of pore sizes significantly larger than 10 m, which are characteristic of such subsurface porous media. As a consequence, increasing the longitudinal dispersion strength in the model corresponds to increasing the grain size in dimensional units. This choice of dimensionalization is different from the one used by Hidalgo et al.¹⁴ who used the total diffusion $D_0 + \alpha_L u^*$ instead of D_0 to define the Rayleigh number; this difference in non-dimensionalization scheme will be further discussed in section IV A.

Convective dissolution of Carbon Dioxide in porous media: impact of dispersion

C. Initial condition

The initial condition to be applied to such a model has been the topic of numerous debates regarding its feasibility and realistic implications. It was delineated that instability structures that are triggered by the propagation of numerical errors may not match experimental results³². Such an observation follows from the fact that any pore-scale flow will experience continuous perturbations³³ that will lead to an occurrence of instability much before that predicted by numerical simulations where perturbations originate from numerical errors. Other studies have shown that the time of introduction of perturbation has no effect on the nonlinear onset time provided the perturbations are introduced relatively early^{34,35}. Here we follow the usual procedure for instability initiation in this type of numerical simulations^{5,13,16,36–38} to ensure the validity of the above points. We first consider the background diffusive form, which is invariant in transverse directions and reads as

$$\tilde{c}_b(\tilde{y}, \tilde{t}) = 1 - \frac{4}{\pi} \sum_{n=1}^{\infty} \frac{1}{2n-1} \sin((n-1/2)\pi\tilde{y}) \exp(-(n-1/2)^2\pi^2\tilde{t}/Ra) . \quad (9)$$

It is devoid of dispersion since at initial times the velocity remains negligibly low. We then superimpose to this diffusive form, at time \tilde{t}_p , a perturbation in the form (in 2D)

$$\tilde{c}_p = \mathbb{R} \xi \exp(-\xi^2) \quad \text{with} \quad \xi = \tilde{y} \sqrt{\frac{Ra}{4\tilde{t}_p}} , \quad (10)$$

where $\mathbb{R} = \mathbb{R}(x)$ is a uniformly distributed random number with mean 0.5, which is kept the same throughout all the simulations, and \tilde{t}_p is the time at which the perturbations are introduced. For the 3D scenario, the form of the perturbation is similar with $\mathbb{R} = \mathbb{R}(x, z)$. All simulations are performed with $\tilde{t}_p = 0.01$, thereby ensuring that the nonlinear onset time is much larger than the time at which perturbations are introduced for the given Ra used in the study. Therefore, the net initial condition reads $\tilde{c}_0 = \tilde{c}_b + \varepsilon \tilde{c}_p$ with ε the amplitude of the perturbation. Note that since two systems with same values for $\tilde{t}_p Ra$ and $\varepsilon \sqrt{Ra}$ are equivalent⁴, we have kept the value of \tilde{t}_p and ε (set to 0.01) constant throughout the study.

Convective dissolution of Carbon Dioxide in porous media: impact of dispersion

D. Stream function formulation

1. 2D geometry

A stream function formulation to Eqs. (5) and (7) can be used to reformulate the following equations of the stream function $\psi^{4,5}$:

$$\begin{aligned}\nabla^2 \psi &= \frac{\partial \tilde{c}}{\partial \tilde{x}} \\ \frac{\partial \tilde{c}}{\partial \tilde{t}} + \tilde{\mathbf{u}} \cdot \tilde{\nabla} \tilde{c} &= \frac{1}{Ra} \tilde{\nabla} \cdot (\tilde{\mathbf{D}} \cdot \tilde{\nabla} \tilde{c}),\end{aligned}\quad (11)$$

where the dependence of $\tilde{\mathbf{D}}$ on the velocity is given by Eq. (7). The velocities are derived from the stream function according to

$$\tilde{u}_x = -\frac{\partial \psi}{\partial \tilde{y}}, \quad \tilde{u}_y = \frac{\partial \psi}{\partial \tilde{x}}, \quad (12)$$

and thus satisfy the continuity equation.

The stream function ψ must be constant at the top and bottom boundaries of the flow domain, with the same value on both boundaries (otherwise there would be a global horizontal flow rate in the system). That (gauge) value, however, is arbitrary. At the lateral (vertical) boundaries the stream function is periodic. The boundary conditions for \tilde{c} are the following:

$$\tilde{c}(\tilde{x}, 0, \tilde{t}) = 1, \quad \frac{\partial \tilde{c}}{\partial \tilde{y}}(\tilde{x}, 1, \tilde{t}) = 0 \quad \text{and} \quad \tilde{c}(0, \tilde{y}, \tilde{t}) = \tilde{c}(\tilde{L}, \tilde{y}, \tilde{t}), \quad (13)$$

with $\tilde{L} = L/H$.

2. 3D geometry

Similarly, a stream formulation can be applied to Eq. (5) and (7) in a 3D flow domain³⁹. The velocity field is inferred from the stream function through

$$\tilde{u}_x = \frac{\partial \psi}{\partial \tilde{y}}, \quad \tilde{u}_y = -\frac{\partial \psi}{\partial \tilde{x}} - \frac{\partial \theta}{\partial \tilde{z}}, \quad \tilde{u}_z = \frac{\partial \theta}{\partial \tilde{y}}, \quad (14)$$

and thus satisfies the continuity equation. The stream function is found by solving the following equations:

$$\begin{aligned}\nabla^2 \theta - \frac{\partial^2 \theta}{\partial \tilde{x}^2} + \frac{\partial^2 \psi}{\partial \tilde{x} \partial \tilde{z}} &= -\frac{\partial \tilde{c}}{\partial \tilde{z}} \\ \nabla^2 \psi - \frac{\partial^2 \psi}{\partial \tilde{z}^2} + \frac{\partial^2 \theta}{\partial \tilde{x} \partial \tilde{z}} &= -\frac{\partial \tilde{c}}{\partial \tilde{x}} \\ \frac{\partial \tilde{c}}{\partial \tilde{t}} &= \tilde{\mathbf{u}} \cdot \tilde{\nabla} \tilde{c} = \frac{1}{Ra} \tilde{\nabla} \cdot (\tilde{\mathbf{D}} \cdot \tilde{\nabla} \tilde{c})\end{aligned}\quad (15)$$

Convective dissolution of Carbon Dioxide in porous media: impact of dispersion

where again the dependence of $\tilde{\mathbf{D}}$ on the velocity field is given by Eq. (7).

The stream functions θ and ψ must be constant at the top and bottom boundaries of the flow domain, with the same value on both boundaries (otherwise there would be a global horizontal flow rate in the system). That (gauge) value, however, is arbitrary. At the lateral (vertical) boundaries the stream functions are periodic. The boundary conditions for \tilde{c} are

$$\begin{aligned} \tilde{c}(\tilde{x}, 0, \tilde{z}, \tilde{t}) = 1, \quad \frac{\partial \tilde{c}}{\partial \tilde{y}}(\tilde{x}, 1, \tilde{z}, \tilde{t}) = 0, \quad \tilde{c}(0, \tilde{y}, \tilde{z}, \tilde{t}) = \tilde{c}(\tilde{L}, \tilde{y}, \tilde{z}, \tilde{t}), \\ \text{and } \tilde{c}(\tilde{x}, \tilde{y}, 0, \tilde{t}) = \tilde{c}(\tilde{x}, \tilde{y}, \tilde{L}, \tilde{t}). \end{aligned} \quad (16)$$

E. Numerical Simulations

For the two-dimensional flow domain, we solve the equation set (11) along with the boundary conditions (13). In the three-dimensional domain, the set of governing equations solved are (15), with boundary conditions (16). The equations are solved numerically using the classical fine-volume discretization within the open source CFD toolbox *OpenFOAM*. A Gauss bounded upwind scheme, which is a bounded scheme⁴⁰, is used for the discretization of the divergence terms, while the Laplacian terms are discretized using a Gauss linear corrected scheme, both of which are second-order accurate. The latter uses Gauss theorem to convert the volume integral to surface integral and then compute the surface fluxes using the given interpolating schemes. To maintain order consistency, the time is discretized using the classical bounded backward implicit scheme. With these numerical schemes, we have developed a fully two-way coupled Darcy-Transport equation solver within *OpenFOAM* for both 2D and 3D cases wherein the stream function equations are solved using the Preconditioned conjugate gradient (PCG) solver with Diagonal-based Incomplete Cholesky (DIC) preconditioner. The transport equation is solved using the stabilized Preconditioned bi-conjugate gradient with Diagonal-based Incomplete LU (DILU) preconditioner. A convergence tolerance of 10^{-6} is used all throughout the simulation.

For the 2D flow domain, a rectangular domain with $L = 3H$ (i.e., an aspect ratio of 3) and a grid size 1000×1000 are used. The aspect ratio is chosen so that the widest convection structure remains sufficiently small in comparison to the flow domain's lateral size for all considered parameter combinations. The grid size is similar to those chosen by a number of earlier studies addressing Rayleigh numbers in the same range. It was chosen sufficiently large for the inferred nonlinear onset time and mean solute concentration not to be impacted by the grid size (the latter over large time ranges) for $Ra = 3000$; see Appendix A for more details. We did not seek to

Convective dissolution of Carbon Dioxide in porous media: impact of dispersion

TABLE I. Values used in the parametric study for the Rayleigh number Ra , the strength of longitudinal dispersion S , the dispersivity ratio α , the flow domain's aspect ratio, and the grid size.

Parameters	Values (2D)	Values (3D)
Ra	1000, 3000	1000, 3000
S	0, 1, 20, 50	0, 20, (50 for $Ra = 3000$ & $\alpha = 0.1$)
α	0, 0.1, 0.3, 0.5	0, 0.1, (0.3 and 0.5 for $Ra = 3000$ & $\alpha = 0.20$)
Aspect ratio of flow domain	3	1
Grid size	1000 \times 1000	250 250 400 ($Ra = 1000$)
		350 350 600 ($Ra = 3000$)

optimize the grid size when investigating $Ra = 1000$, and thus kept it at the same value as for $Ra = 3000$.

For the 3D simulations, we use a cubic domain ($L = H$) with grid size $250 \times 250 \times 400$ for $Ra = 1000$ and $350 \times 350 \times 600$ for $Ra = 3000$. Such grid sizes are as large as, or significantly larger than, the grid sizes used by earlier 3D studies (see, e.g., Hewitt, Neufeld, and Lister¹⁸). Note that these did not consider hydrodynamic dispersion, but accounting for dispersion does not require a finer grid, since it results in an increase in the finger width as compared to the same configuration with only molecular diffusion.

For all the simulations, the domain is decomposed into smaller sections and the whole solver is parallelized across 8 logical cores for faster implementation. The initial dimensionless Δt is chosen as 10^{-7} and a gradual time-adaptative scheme with maximum $\Delta t = 0.01$ is used based on the iterations needed to converge a particular set of coupled equations, thereby speeding up the overall solution process.

The model and numerical codes were validated by comparison to data from Tilton, Daniel, and Riaz⁶, as explained in Appendix B.

The values used in the parametric study of section III for the various parameters defining the flow configuration are given in Table I.

Convective dissolution of Carbon Dioxide in porous media: impact of dispersion

F. Scalar quantities of interest

From the simulated concentration and velocity fields, we analyze the impact of the strength of longitudinal dispersion S , its anisotropy α , and the Rayleigh number Ra on six scalar observables. Firstly, the penetration depth of solute fingers is defined at any given time as the mean vertical position of the $\tilde{c} = 0.25$ iso-concentration line. Secondly, the finger number density, i.e., the number of fingers within a transverse linear unit length can be estimated at any time using from iso- \tilde{c} plots, counting the number of region of maxima encountered (see for example in 3D Fig. 3).

Thirdly, the nonlinear onset time of the instability is the time at which the temporal evolution of the total vertical solute flux starts to be impacted by the existence of convection, thus deviating from the decreasing behavior attached to the purely-diffusive concentration profile (9) and exhibiting a first trough that marks the nonlinear onset time of instability. At the top boundary of the flow domain, which is horizontal (i.e., we assume a flat geometry of the scCO₂-solution interface), the velocities are horizontal and therefore the vertical solute flux is purely diffusive (no advective flux), but it is still impacted by convective velocities due to the dependence of the dispersion tensor on them. The dimensionless form of the flux reads in 2D as

$$\tilde{J}(\tilde{t}) = \frac{1}{Ra} \int_{\tilde{x}=0}^{L/H} (1 + S \|\tilde{\mathbf{u}}(\tilde{x}, 0, \tilde{t})\|) \left. \frac{\partial \tilde{c}}{\partial \tilde{y}} \right|_{\tilde{y}=0} d\tilde{x}, \quad (17)$$

the 3D formulation involving a second integration over \tilde{z} between 0 and L/H . Note that the dissolution flux is often normalized in the literature by its value in the absence of convection, yielding what is termed the Sherwood number. We have chosen not to investigate that observable.

We also compute the average CO₂ concentration in the flow domain, which in 2D is obtained as

$$\bar{c}(\tilde{t}) = \frac{1}{A_\Omega} \int_\Omega \tilde{c}(\tilde{\mathbf{x}}, \tilde{t}) d\tilde{\mathbf{x}}, \quad (18)$$

where Ω is the total flow domain, and A_Ω is its area (in 2D, or volume in 3D).

Finally, we compute a measure of the mixing capacity within the liquid phase in the form of the scalar dissipation rate, the dimensionless form of which is^{41,42}

$$\chi(\tilde{t}) = \frac{1}{A_\Omega} \int_\Omega \left(\tilde{\mathbf{D}} \cdot \tilde{\nabla} \tilde{c}(\tilde{\mathbf{x}}, \tilde{t}) \right) \cdot \tilde{\nabla} \tilde{c}(\tilde{\mathbf{x}}, \tilde{t}) d\tilde{\mathbf{x}}. \quad (19)$$

The scalar dissipation rate is expected to approach zero at infinite times. At early times corresponding to the diffusive regime (before convection sets in), $\tilde{\chi}$ behaves as an inverse square root of time in the form $(1/4)\sqrt{\pi Ra/(2t)}$, and is thus proportional to the diffusion flux $\tilde{J} = 1/\sqrt{4Ra t}$.

Convective dissolution of Carbon Dioxide in porous media: impact of dispersion

More generally, $\tilde{\chi}$ and \tilde{J} are related by the following relation, derived by adapting Eq. (4) in Ref.⁴³ to our non-dimensionalization scheme:

$$\frac{d\langle c^2 \rangle}{dt} = 2 \left(\frac{\tilde{J}}{L/H} - \frac{\tilde{\chi}}{Ra} \right), \quad (20)$$

where $\langle c^2 \rangle$ is the second (non-centered) moment of the concentration distribution. In contrast to Rayleigh-Taylor-Darcy configurations for which the mean concentration remains constant in time, during convective dissolution $\langle c^2 \rangle$ is finite and varies in time, so that no a priori relation can be inferred between $\tilde{\chi}$ and \tilde{J} .

III. RESULTS

We first investigate how the concentration and velocity fields are impacted, in terms of penetration depth, finger number density and maximum velocity; then we analyze the behavior of the total dissolution flux, nonlinear onset time, mean concentration and scalar dissipation rate.

A. Phenomenology of the flow

Fig. 2 shows the concentration (left column) and velocity (right column) fields for two values of the Rayleigh number, $Ra = 1000$ and $Ra = 3000$ at a given time ($\tilde{t} = 10$ and 6, respectively), and for various configurations of the dispersion tensor. As reported in numerous previous experimental and numerical studies, the finger number density (FND), or wavenumber, is observed to increase with the Rayleigh number, i.e. between Fig. 2a and 2g, 2b and 2h, as well as 2c and 2i. When comparing the case of no mechanical dispersion ($S = 0$) to that with a strong dispersion ($S = 50$) and dispersivity ratio $\alpha = 0.1$ typical of many sedimentary subsurface formations, the FND of the gravitational fingers is smaller for a larger longitudinal dispersion strength (see Fig. 2g and 2h), and the same holds for the penetration depth of the fingers; this behavior is more pronounced for $Ra = 3000$ than for $Ra = 1000$. This is consistent with the stronger mixing associated with the larger effective diffusion coefficient resulting from mechanical dispersion. However, for a higher dispersivity ratio ($\alpha = 0.5$), i.e. a stronger transverse dispersivity, the finger penetration is larger than for $\alpha = 0.1$ (see Fig. 2c vs. 2b and 2i vs. 2h), but only marginally so (see Appendix D), while the finger density number is not much impacted. But the fingers are still less advanced towards the bottom of the flow domain when mechanical dispersion is present, whatever the dispersivity ratio may be, as seen when comparing Fig.2a with 2c or Fig. 2g with Fig. 2i.

Convective dissolution of Carbon Dioxide in porous media: impact of dispersion

Considering now the 3D geometry, this behavior is also observed on iso-surfaces $\tilde{c} = 0.25$ of the 3D concentration, as depicted at time $\tilde{t} = 4$ in Fig. 3 for longitudinal dispersion strengths $S = 0$ and $S = 20$. The finger number density is all the larger as the Rayleigh number is larger, as expected. Furthermore, the convection exhibits thicker and more round-shaped fingers when dispersion is significant, as compared to the case without hydrodynamic dispersion. As also observed in the 2D geometry (Fig. 2), with a larger dispersion the finger penetration depth within the system is smaller.

The latter conclusion relative to the penetration depth at a given non-dimensional time is confirmed by Fig. 4: increasing the Rayleigh leads to slower penetration, and so does an increase in hydrodynamic dispersion (in comparison to pure molecular diffusion) with a rather standard dispersivity ratio of $\alpha = 0.1$. Let us now examine vertical profiles of FND for various combinations of Ra numbers and longitudinal dispersion strengths S (Fig. 5). The figure confirms the qualitative observation of Figs. 2 and 3. At a given time, the FND decreases with the vertical coordinate due to transverse coalescence of the solute fingers. Note that the vertical FND profile flattens in time (not shown here), as the large FND near the top boundary of the domain decreases while the penetration depth of the fingers increases. This has been previously observed in numerous experiments (e.g, Wang *et al.*¹¹, Fernandez *et al.*⁴⁴, Nakanishi *et al.*⁴⁵). The FND is always larger at any vertical position for $Ra = 3000$ than for $Ra = 1000$ (Fig. 5a and 5c). However, with an increase in hydrodynamic dispersion within the medium, increased transverse dispersion accelerates finger coalescence as concentration fingers progress towards the bottom of the flow domain. For a given Ra number, an increase in dispersion S thus results in a smaller finger number density (Fig. 5). For $Ra = 1000$ this difference is significant at small times but decreases with time, whereas for $Ra = 3000$ the impact of dispersion (as compared to the pure molecular diffusion case) increases in time. These observations remain persistent across different values of the dispersivity ratio α , which has little impact on the finger number density (see Appendix D).

The velocity fields shown in the lower panel of Fig. 2 for the same flow conditions as the concentration fields shown in the upper panel of the same figure, reflect the convective strength of the instability process. The dependence of the mechanical dispersion on the local velocity magnitude introduces an additional coupling between velocities and concentrations: higher velocity magnitudes incur a higher impact of dispersion on the resulting dynamics. A general observation from the velocity maps in the lower panel of Fig. 2 is that the velocity magnitude near the top boundary is small but that a non-zero horizontal component exists, due to the slip condition

Convective dissolution of Carbon Dioxide in porous media: impact of dispersion

imposed on velocity at the top boundary of the domain, which corresponds to the free surface between supercritical CO₂ and the aqueous phase (see the maps of \tilde{v}_x in Fig. 19a in Appendix C). This tangential velocity field at the wall also contributes to the net dispersive flux through Eq. (7). The velocity profile also exhibits alternating regions of high and low magnitudes, and the general structure reflects that of the concentration maps, with thinner fingers for a larger Rayleigh. The high magnitude regions are signatures of faster penetrating downward fingers, as well as of regions where the resident fluid comes up to replace the mixture near the top boundary of the domain. Unsurprisingly, boundaries between those regions of downward and upward flow exhibit a very low velocity. Comparing plots (d), (e) and (f) in the lower panel of Fig. 2, we investigate the impact of hydrodynamic dispersion on the spatial distributions of the velocity magnitude. The slow-down of descending fingers by dispersion is obvious for $\alpha = 0.1$ (Fig. 2e), with thinner and shorter fingers (see also the \tilde{v}_z maps in Fig. 19a in Appendix C)) and lower velocity magnitudes as compared to the configuration with no dispersion (Fig. 2d), especially in the region just below the top domain boundary. In contrast, for $\alpha = 0.5$ (Fig 2f), the velocity maps show much broader fingers than for $\alpha = 0.1$ (Fig 2e).

The temporal evolution of the largest velocity in the 2D domain is shown in Fig. 6 for $Ra = 1000$ and $Ra = 3000$, and for three dispersion configurations. For $Ra = 3000$, and for all dispersion configurations, the largest velocity reaches some sort of plateau around which it fluctuates, while for $Ra = 1000$ we expect it to behave in the same way but the plateau is hardly reached at our maximal simulation time, $\tilde{t} = 10$, for $S = 50$. The fluctuations are likely related to the merging of convection fingers. As also reported previously^{29,31}, this plateau of the finger penetration velocity does not vary drastically with dispersion. Hydrodynamic dispersion slows down the transitory regime before the plateau is reached, but the dispersivity ratio α seems to have little impact. Note that we do not show the corresponding plots obtained in the 3D domain, as the maximal investigated time is $\tilde{t} = 4$ for the 3D data, which is a bit early to conclude on the maximal velocity behavior.

B. Flux and onset time

In light of these observations, the flow structure and concentration field are obviously strongly influenced by the strength of longitudinal hydrodynamic dispersion as well as the medium's anisotropy. Therefore, we expect these quantities to impact the onset of convection and the disso-

Convective dissolution of Carbon Dioxide in porous media: impact of dispersion

lution rates in the medium.

Fig. 7 shows the temporal evolution of the flux \bar{J} in the 2D geometry, for different Rayleigh numbers Ra and longitudinal dispersion strengths S , while Fig. 8 shows similar data obtained in the 3D geometry. The flux profile exhibits an initial diffusive regime followed by a minimum which indicates the onset of convection. As expected, the diffusive regime is independent of the Rayleigh number and features a power law scaling as a function of time, in the form $\propto t^{-1/2}$ (see Appendix A). The variation in onset time, when varying the parameters that control hydrodynamic dispersion (S and α), are not drastic, in contrast to what was reported previously by Ghesmat, Hassanzadeh, and Abedi²⁸; but they are significant. We'll discuss in section IV A why our findings differ on this aspect from that of Ghesmat, Hassanzadeh, and Abedi²⁸ and other authors. Comparing the temporal evolution of the fluxes for $Ra = 1000$ and $Ra = 3000$ (i.e., Fig. 7a and 7b to 7c and 7d, respectively), we observe that an increase in Rayleigh number decreases the onset time, as already observed by several studies previously. Considering dispersivity ratios $\alpha = 0.1$ and $\alpha = 0.5$, both at $Ra = 1000$ (Fig. 7b and Fig. 7d) and $Ra = 3000$, and varying the longitudinal dispersion strength between $S = 0$ and $S = 50$, we see that the onset time varies with S but in a manner that depends both on Ra and α . The results are summarized in Fig. 9. For $Ra = 1000$ in the 2D geometry (Fig. 9a), an increase in mechanical dispersion S delays the onset when $\alpha = 0.1$, but for $\alpha = 0.3$ and $\alpha = 0.5$ (more so in the latter case), on the contrary, the onset time is decreased with increasing S . Furthermore, at any investigated S value, increasing the dispersivity ratio decreases the onset time. For $Ra = 3000$ in the 2D geometry (Fig. 9b), a similar trend is observed when changing the dispersivity ratio at a given longitudinal dispersion strength: the onset times decrease with α ; it also decreases monotonically with S for $\alpha = 0.3$ and $\alpha = 0.5$, but for $\alpha = 0.1$ the plot is not monotonic: it decreases between $S = 0$ and $S = 20$, and increases between $S = 20$ and $S = 50$. The temporal evolution of the flux in 3D cases shows a behavior consistent with the 2D observations: for $Ra = 1000$ and $\alpha = 0.1$, increasing S delays the onset of convection, while for $S = 20$ increasing α leads to a smaller onset time. The results obtained in the 3D geometry are summarized in Fig. 9c for $Ra = 1000$; the dependence on dispersion parameters is consistent with the results obtained for the equivalent configuration in 2D (Fig. 9a). Furthermore, when comparing the onset times obtained in the 2D and 3D geometry, all parameters being identical otherwise, the onset is observed to occur slightly earlier in the 3D geometry. This difference between onset times in the 2D and 3D geometries seems all the more apparent as the Ra number is smaller (see Fig. 8a vs. Fig. 8b).

Convective dissolution of Carbon Dioxide in porous media: impact of dispersion

Besides the variation in the onset time, a large impact of hydrodynamic dispersion is observed after the convective instability kicks in. The overall flux in the constant flux regime, where the flux oscillates around a plateau that is more clearly defined, and over a larger time range, for higher Rayleigh numbers (Emami-Meybodi *et al.*⁷, see Fig. 7c and 7d as compared to 7a and 7b, respectively) tends to decrease slowly with time. Nevertheless, that plateau flux remains higher than the pure diffusive flux, and is slightly larger for $Ra = 1000$ than for $Ra = 3000$. It is also reached earlier for $Ra = 3000$ than for $Ra = 1000$, as the onset time is lower in the latter case. The impact of the dispersion parameters on the plateau is qualitatively similar for the two investigated Rayleigh values. At a given Rayleigh number, increasing the longitudinal dispersion's strength at $\alpha = 0.1$ decreases the mean flux in the constant flux regime, while for $\alpha = 0.5$ the opposite behavior is observed.

C. Mean concentration

After the nonlinear regime is established, the evolution in the flux profile fluctuates widely, as previously discussed. Thus, though the total mass of solute is the integral in time of the flux, it is not obvious how the flux evolution with time translates into the evolution of the mean concentration \bar{c} inside the flow domain, which is the most straightforward measure of the advancement of dissolution trapping of CO_2 inside the geological formation and is also the time primitive of the flux.

Fig. 10a shows the evolution of \bar{c} in the 2D geometry as a function of time for $Ra = 1000$ and $Ra = 3000$, $\alpha = 0.1$ and $\alpha = 0.5$, and values of S ranging between $S = 0$ and $S = 50$. As seen previously on the onset time, at any given time an increase in S for $\alpha = 0.1$ leads to a decrease of the mean concentration, while for $\alpha = 0.5$ it leads on the contrary to an acceleration of the dissolution. Increasing α also leads to a larger average growth rate. At the larger Rayleigh, the growth is also quicker than at the lower Rayleigh. These dependences on the Rayleigh and dispersion parameters are summarized in Fig. 11, which shows \bar{c} as a function of the dispersivity ratio for different longitudinal dispersion strengths, both for $Ra = 3000$ and $Ra = 1000$. For $\alpha = 0.1$ and $Ra = 3000$ the dependence on S is non-monotonic, and for $S \geq 20$ the dependence on α is also non-monotonic, for both $Ra = 3000$ and $Ra = 1000$. In summary, the mean concentration evolution seems to be consistent with, and, possibly, mostly controlled by, the behavior of the onset time: a configuration that exhibits a larger onset time will get a head start and keep in time.

Convective dissolution of Carbon Dioxide in porous media: impact of dispersion

Comparison of the data obtained in the 3D and 2D geometries (Fig. 12) for $Ra = 1000$ shows that the effective dissolution, as measured by the time evolution of \bar{c} , is somewhat faster in the 3D system (by less than 15%), with a peak in the relative difference occurring at a time at which the 3D convection has already started while the 2D convection hasn't. Unfortunately our comparison addressed only non-dimensional times smaller than 4, due to the high computational time of the 3D simulation.

D. Scalar dissipation rates

The scalar dissipation rate (SDR) is a global measure of how strong mixing is within the flow domain, which is controlled by the intensity of concentration gradients in the system. As mentioned at the end of section II F, its definition resembles that of the diffusion flux, but these two quantities cannot be expected to be related in a simple straightforward manner during convective dissolution, except during the initial diffusive regime. Fig. 13 shows its temporal evolution in the 2D geometry, for different parameter configurations. In particular, Fig. 13a addresses the behavior of the scalar dissipation for different strengths S of the longitudinal dispersion, with $Ra = 1000$ and $\alpha = 0.1$; the configurations are exactly identical to those of Fig. 7a, and the different plots corresponding to the same configurations in the two figures exhibit a strong correlation. In other words, the overall strength of mixing in the entire flow domain is strongly correlated with the dissolution flux at the top boundary of the domain, at least at this Rayleigh number, $Ra = 1000$. The expected initial $-1/\sqrt{t}$ (not shown here), proportional to that of the dissolution flux (see section II F), is observed at early times. After the convection sets in, similarly to the dissolution flux, the SDR is observed to increase sharply, and then fluctuates more or less strongly around a stationary or slowly decreasing tendency. The time at which the minimum value of the SDR is observed, is directly related to the onset time defined from the minimum of the dissolution flux's, and its dependence on Ra , S and α thus follows the same behavior as discussed above (section III B). For a dispersivity ratio of $\alpha = 0.1$ and at $Ra = 1000$, introducing dispersion ($S > 20$ vs. $S \sim 0$) induces a weak decrease in the SDR (Fig. 13b), which is consistent with what was observed for the dissolution flux. For $S = 20$ and at $Ra = 1000$, an increase in the dispersivity ratio increases the SDR in the fluctuation regime as soon as $\alpha > 0$ (Fig. 13b). However, a system with no dispersion seems to mix as well as the configuration with $S = 20$ and $\alpha = 0.3$.

Fig. 13c shows the same dispersion configurations as Fig. 13b, except that the Rayleigh value

Convective dissolution of Carbon Dioxide in porous media: impact of dispersion

is larger in the former ($Ra = 3000$) than in the latter ($Ra = 1000$). Here, in contrast to what was observed for the dissolution rate, a larger Rayleigh induces a significantly larger SDR. This is confirmed by Fig. 13d, where the temporal evolution of the SDR is shown for the two investigated Rayleighs and for a dispersion that is either non-existent or defined by $S = 20$ and $\alpha = 0.3$. We conclude that increasing the Rayleigh does increase the concentration gradients, as expected due to the larger density contrast between the CO_2 -enriched solution and that which is devoid of CO_2 , and thus strengthens the mixing, but also leads to stronger convection, which, by advection, tends to restrict the occurrence of strong concentration gradients to smaller regions at the boundaries between downward flow and upward flow; these two antagonistic effects seem to balance each other so that the dissolution rate in the fluctuating regime is not much influenced by the Rayleigh (see section III B). But of course the Rayleigh number strongly impacts the onset time of convection, which we have discussed above (this is well known from the literature).

Fig. 14a is identical to Fig. 13a, except that it was obtained in the 3D geometry. It exhibits a behavior fully consistent with that of its 2D counterpart. In Fig. 14b, the temporal evolution of the SDR are shown for $S = 20$ and $\alpha = 0.1$ and for the two investigated Rayleigh numbers, obtained either in the 2D or in the 3D geometry. These plots confirm that the dimensionality of space has little impact on the SDR, but that the SDR is all the larger as the Rayleigh is larger.

E. Long term behavior of convective dissolution

We now examine how convective dissolution behaves in term of the scalar dissipation rate (Fig. 15), total dissolution flux (left inlet in Fig. 15), and mean concentration (right inlet in Fig. 15) at large times. These temporal evolutions over non-dimensional times as large as 70 could only be obtained in the 2D geometry, due to obvious constraints of computational times. They are plotted for $Ra = 1000$ and $S = 20$ and for various dispersivity ratios. At large times (i.e., in the shutdown regime), the disparity due to differences in dispersivity ratios, introduced in the dynamics after the initiation of convection, tend to diminish, as observed from the converging dissolution flux and scalar dissipation rates. This is expected since, as convection shut downs, fluid velocities decrease and thus render the impact of dispersion insignificant. Nevertheless, the impact of the dispersion on the onset time of convection and on the constant dissolution flux in the constant flux/fluctuation regime is clearly seen in the temporal evolution of the mean concentration, which is essentially a temporal primitive of the dissolution flux. The discrepancies in \bar{c} are introduced in the constant

Convective dissolution of Carbon Dioxide in porous media: impact of dispersion

flux regime and cease to increase at large times, but remain. The net dissolved mass depends monotonically on the dispersivity ratio and is largest for $\alpha = 0.5$, which features the smallest non-linear onset time and the largest peak in the dissolution flux and scalar dissipation curves. These conclusions remain valid across a range of different configurations of Ra values and dispersion parameters, which are not shown here.

IV. DISCUSSION

A. Impact of dispersion on convective dissolution

1. Summary of our findings:

From the results presented above, we can draw the following synthesis regarding the impact of hydrodynamic dispersion on convective dissolution:

a. Impact on convection structure: The presence of mechanical dispersion, irrespective of the dispersivity ratio, works towards decreasing the finger number density (FND) of the ensuing fingers, at any time and any vertical coordinate at which at least one finger exists. The penetration depth, as defined by an iso-concentration line (2D geometry) or surface (3D geometry) is also smaller with mechanical dispersion than with molecular diffusion alone. These two observations can both be related to the role of transverse dispersion, which favors transverse coalescence of concentration fingers, thus contributing to decreasing the FND, and may tend to homogenize the concentration field, thus slowing down the convection which is driven by density contrasts resulting from concentration contrasts. Note however that for a given amplitude of the longitudinal dispersion, increasing the transverse dispersion has little impact on the finger number density. Such observations on the penetration depth have previously been made by Menand and Woods³⁰, while similar observations on the finger structure have previously been reported experimentally by Wang *et al.*¹¹, who imaged 3D granular bead packs by X-ray tomography and used three different sizes of bead to vary the dispersivity length of the granular porous medium.

Considering the same parameters as Wang *et al.*¹¹ in order to compare our numerical results to their experimental measurements, i.e. $Ra = 3000$, $K = 2.63 \times 10^{-10} \text{ m}^2$, $\phi = 0.5$, $g = 9.81 \text{ m}^2 \text{ s}^{-1}$, $\eta = 0.001115 \text{ Pa s}$, $\Delta\rho = 14 \text{ kg m}^{-3}$, $D_0 = 2 \times 10^{-9} \text{ m}^2 \text{ s}^{-1}$, $\alpha_L = 10^{-3} \text{ m}$, $U^* = K\Delta\rho g/\eta$, $S = \alpha_L U^*/D = 20$, $H = \eta\phi DRa/(K\Delta\rho g) = 11 \text{ cm}$, we obtain a FND of order $0.5 \text{ N}\cdot\text{cm}^{-2}$ or less, in good agreement with the measurements presented in the experimental study. Although our

Convective dissolution of Carbon Dioxide in porous media: impact of dispersion

simulations are performed with periodic boundary configuration, the effect of lateral confinement on the ensuing FND does not seem to strongly impact the result.

b. Impact on finger velocity and penetration depth: Hydrodynamic dispersion slows down the establishment of the finger velocity as compared to molecular diffusion alone. This translates in terms of the penetration length at a given non-dimensional time, which is less when hydrodynamic dispersion exists than without it. In the constant flux regime observed at sufficiently large Rayleigh, due to the large fluctuations around the long time tendency, it is not obvious from our current numerical data if the ratio of the transverse to the longitudinal dispersivity of the medium impacts the convection velocity.

c. Impact on nonlinear onset time: Previous numerical studies on the impact of dispersion on convective dissolution^{14,28} have brought forth that the onset time decreases with the longitudinal dispersion strength S . In contrast to these studies, we observe that the dependence of t_{on} on S is not necessarily monotonous, and that in addition it depends both on the Rayleigh number and on the dispersivity anisotropy α . At dispersivity ratios typical of subsurface formations ($\alpha \simeq 0.1$), the onset time increases with longitudinal dispersion strength. At larger dispersivity ratios, the onset times increases more slowly with S and can even decrease with S if α is sufficiently large (e. g., $\alpha = 0.5$). For an intermediate value of α and for a sufficiently large Rayleigh, the dependence of t_{on} on S can be non-monotonic, due to competition between the two latter effects.

This non-monotonicity as a function of S at fixed α seems to indicate that the (S, α) space is perhaps not that in which the physics at play appears the most clearly. In Fig. 16 we plot the variations of the non-linear onset time in the $(S, S\alpha)$ space, where the two axes are non-dimensional representations of the longitudinal and transverse dispersion coefficients, respectively. Iso- α lines are shown as black straight lines. From this plot it appear clearly when considering the dependence of the nonlinear onset time on the longitudinal dispersion at constant transverse dispersion (rather than constant α) that increasing the longitudinal dispersion slows down the convection, while at constant longitudinal dispersion increasing the transverse dispersion accelerates it.

In most natural systems as well as granular porous media prepared in the laboratory, however, the dispersivity ratio is close to 0.1 (solid black line in Fig. 16), so we should expect hydrodynamic dispersion to act to increase the onset time and thus act as a hindrance to convective dissolution. Note also that in the real world the dispersivity length scales with the typical grain size of the porous medium, a , and the Rayleigh number scales with the permeability, which scales as a^2 . We discuss the link between our findings, those of previous numerical simulations, and those of

Convective dissolution of Carbon Dioxide in porous media: impact of dispersion

experimental studies in section IV A 2 below.

d. Impact on constant flux regime: The longitudinal dispersion strength also impacts the constant flux regime, which would be probably more well-established if the Rayleigh number were of order 10^4 rather than 1000 as investigated here. Nevertheless, the longitudinal dispersion strength has a clear effect on the mean flux, and that effect is strongly impacted by the dispersivity ratio: at $\alpha = 0.1$ increasing the longitudinal dispersion strength decreases the value slightly, while at $\alpha = 0.5$ a much more significant increase of the mean flux value is observed when increasing S .

e. Impact on mean concentration: The combined impact of the onset time and mean plateau flux on the overall dispersion of CO_2 in the liquid phase is captured by the time evolution of the mean CO_2 concentration \bar{c} . At a time well into the constant flux regime, the behavior of the mean concentration as a function of S and α is fully consistent with that of the onset time, which shows that the main control on the overall dissolution is the onset time rather than the plateau value. This is consistent with our observations on the long time behavior convection dissolution, where the global dissolution is seen to be controlled by the time scale of the convection's initiation. The impact of the dispersivity ratio on the mean concentration, in particular, is exactly opposite to that on the onset time, as a larger onset time translates into a smaller mean concentration at any given time after the convection has kicked in. Thus, a higher α translates into a stronger convective dissolution. This can be attributed to the fact that stronger transverse dispersion corresponds to a greater capability of the fingers to mix with the resident fluid, as evidenced by the temporal evolution of the scalar dissipation rate. These findings are consistent with those of De Paoli²⁷, who also found that transverse dispersion is an important control factor in the early stages of dissolution.

Considering the standard value of 0.1 for the dispersivity ratio, however, leads to a decreasing behavior of the mean concentration as a function of the longitudinal dispersion strength, at any given time into the constant flux regime. Therefore, for most natural formations and porous media prepared in the laboratory, one would expect hydrodynamic dispersion to hinder the efficiency of convective dissolution. This is in stark contrast with the common view brought forth by previous numerical studies^{14,28}; we shall now discuss this discrepancy.

Convective dissolution of Carbon Dioxide in porous media: impact of dispersion

2. *How do our results compare to those of previous numerical and experimental studies ?*

Generally, numerical investigations (e.g., Hidalgo and Carrera¹⁴, Ghesmat, Hassanzadeh, and Abedi²⁸) so far have claimed that hydrodynamics dispersion acts towards accelerating convective dissolution by lowering the nonlinear onset time. As mentioned above, for many natural porous media the anisotropy ratio is close to 0.1, for which our model predicts an increasing dependence of the onset time on longitudinal dispersion strength. So why have previous numerical simulations predicted the contrary for similar configurations ? It is due to the way those numerical studies have non-dimensionalized the governing equations: it leads to their Rayleigh number being dependent on the longitudinal dispersion strength, so that increasing the dispersion strength in the non-dimensionalized simulation (while maintaining the medium's porosity and permeability constant) results effectively in also increasing the Rayleigh number, which is $Ra' = Ra/(1 + S')$ with $S' = S/(1 + S)$, where Ra and S are the Rayleigh number and dispersion strength defined in the present study (see more details in Appendix E). In that case the increases in S and Ra play antagonistic roles, but the increase in Rayleigh number, which tends to decrease the nonlinear onset time, easily dominates. On the contrary, in the present numerical study S and Ra are two independent parameters. More details on the impact of the non-dimensionalization scheme on the apparent role of dispersion are given in Appendix E. On the contrary, the numerical study of Wen, Chang, and Hesse²⁶ decorrelates the longitudinal dispersion's strength (our parameter S) from the standard, diffusive, Rayleigh number (which is the one we consider), by introducing a second, dispersive, Rayleigh number, which is proportional to our S . However, these authors have not investigated the nonlinear onset time. In addition, they have used a Dirichlet boundary condition at the bottom of the flow domain, which is not relevant to the convective dissolution of CO₂.

Few experimental studies have addressed the impact of hydrodynamic dispersion's intensity on convective dissolution, but they have supported a view opposite to that brought forth by numerical studies so far (see e.g., Liang *et al.*⁹, Menand and Woods³⁰). Liang *et al.*⁹ have investigated convective dissolution with analog fluids in granular porous media consisting of glass beads, and measured a mean finger separation (proportional to the inverse of the FND) in the constant flux regime. By changing the size of the glass beads, they scaled the dispersivity lengths of the medium; they observed that the mean finger separation increases as a function of the dispersion strength. Hence they found that the FND decreases with dispersion strength, which is exactly what we observe and is typically associated to a stronger convection resulting from a decrease in the onset

Convective dissolution of Carbon Dioxide in porous media: impact of dispersion

time as a function of the hydrodynamic dispersion. This result is thus in contradiction to the numerical simulation of Ghesmat, Hassanzadeh, and Abedi²⁸ and similar to our numerical findings. Can we then argue that our numerical simulation behave as an experimental study such as that of Liang *et al.*⁹ is expected to ? They do qualitatively, by in fact they are not entirely comparable to such experiments, because increasing the typical grain size a in an increase to increase S does also increase the Rayleigh number Ra because the transmissivity typically grows with a^2 (see e.g. the Kozeny-Carman model Carman⁴⁶); to keep the Rayleigh number constant, the density contrast should be adjusted as well. So when simply changing the grain size, the dispersion strength cannot be increased without increasing the Rayleigh number at the same time, as is the case for the numerical simulation of Ghesmat, Hassanzadeh, and Abedi²⁸. Note however that Liang *et al.*⁹ are aware of this double impact of changing the bead size in the experiment, and analyze their results in terms of the two Rayleigh numbers (diffusive and dispersive) mentioned above. But they cannot decrease the dispersive Rayleigh number (i.e., increase S) without increasing the diffusive Rayleigh number (i.e., our Ra), and vice-versa; so they cannot infer dependent laws for the various properties of the convection process as a function of S at fixed Ra , as the present numerical study has done.

B. Impact of space dimensionality

In the literature a vast majority of the studies of convective dissolution have been performed in 2D setups, either numerically or in experiments. In particular, numerical studies of the impact of dispersion have so far been performed in 2D, while the studies by^{9,11} are to our knowledge the only ones that have addressed the topic experimentally. A handful of numerical studies have presented 3D simulations, but only one has compared 2D and 3D results: Pau *et al.*¹⁷ have shown that increasing the space dimensionality from 2D to 3D results in a slight decrease in onset time and a slight increase in mass flux; note however that these authors do not account for hydrodynamic dispersion in their model. In fact, to our knowledge, only one 3D numerical investigation accounts for hydrodynamic dispersion in its model²⁵, and it does not compare 2D and 3D results.

In this study we have systematically simulated convective dissolution for different sets of parameters (Ra , S , α), both in the the two-dimensional (2D) and three-dimensional (3D) geometries, so as to compare the behaviors of the various observables between 2D and 3D. Due to the heavy computational load associated with 3D simulations, the parameter space has not been described as

Convective dissolution of Carbon Dioxide in porous media: impact of dispersion

completely in 3D as in 2D, but in most cases we have been able to confront the 2D and 3D results. We find that in the absence of dispersion, the finger number density (FND), considered at $\tilde{t} = 4$, is similar at the top of the flow domain between 2D and 3D geometries when $Ra = 1000$, but is larger (by about $\sim 20\%$) in the 3D flow domain when $Ra = 3000$. However, the FND reaches 0 at about the same vertical position as in the 2D flow domain, both for $Ra = 1000$ and $Ra = 3000$. In addition, the impact of dispersion on the vertical FND profiles is similar in 3D and 2D. Accordingly, the temporal evolution of the finger penetration, as defined by the $\tilde{c} = 0.25$ isoline, is very similar in 3D and 2D, whether hydrodynamic dispersion is present or not and for the two investigated Rayleigh number values. The dependence of the onset time on the longitudinal dispersion strength and dispersivity ratio is also similar in 2D and 3D, for the Rayleigh value for which it could be compared ($Ra = 1000$), but the onset time is systematically smaller (by about 20%) in the 3D geometry, in agreement with the previous findings of Pau *et al.*¹⁷. The slight increase in plateau mass flux between 2D and 3D observed by these authors is also confirmed in our numerical simulations, both for $Ra = 1000$ and for $Ra = 3000$.

In conclusion, it seems that the conclusions of Pau *et al.*¹⁷ concerning the impact of space dimensionality, mentioned above, still hold independently of whether hydrodynamic dispersion impacts the convective dissolution process. There is however one qualitative difference between the 3D and 2D numerical simulations: the value of the FND at the top domain boundary, which may differ between 2D and 3D, with a discrepancy depending on the value of the Rayleigh number.

V. CONCLUSION

We have developed a new three-dimensional continuum scale model of convective dissolution that accounts for anisotropic hydrodynamic dispersion. The OpenFOAM CFD package was used to implement the model in a numerical simulation which was then used to investigate systematically the impact of longitudinal dispersion strength (S) and anisotropy ratio (α) on convective dissolution, both in two-dimensional (2D) and in three-dimensional (3D) geometries. We examined in detail how vertical profiles of the number density, the temporal evolution of the fingers' penetration depth, the nonlinear onset time, the dissolution flux after convection has developed, and the temporal evolution of the mean concentration and the scalar dissipation rate, are impacted by S and α ; we also confronted the 2D and 3D findings in each case to see how much they differ. This was done for two Rayleigh numbers: 1000 and 3000.

Convective dissolution of Carbon Dioxide in porous media: impact of dispersion

We find that the overall impact of hydrodynamic dispersion on the efficiency of the convective dissolution process is mostly controlled by its impact on the onset time of convection. In contrast with previous numerical findings, which indicated a strong decrease of the onset time with longitudinal dispersion strength for a standard value of the dispersivity ratio $\alpha = 0.1$, we observe a clear but moderate increase of the onset time with S for $\alpha = 0.1$. This findings is consistent with those of the few experimental studies which have addressed the impact of dispersion, and tends to indicate that hydrodynamic dispersion is expected to be a hindrance to convective dissolution in subsurface formations. This discrepancy with previous numerical findings is due to their non-dimensionalization scheme, which led to the effective Rayleigh number (i.e., the relative strength of molecular diffusion with respect to buoyancy-triggered advection of the solute) being increased when the longitudinal dispersion strength was increased; in our simulation the effective Rayleigh number is independent of the dispersion strength. We also observe that when increasing the dispersivity ratio the dependence of the onset time on the longitudinal dispersion strength changes, with an increasing dependency for $\alpha = 0.5$, and even a non-monotonic behavior at intermediate α values; this dependence $t_{\text{on}}(S, \alpha)$ is actually also impacted by the Rayleigh number. However, when considering the impact of the longitudinal dispersion strength at constant transverse dispersion strength, we observe that the former weakens the convection, and thus, the efficiency of the dissolution process, while on the contrary transverse dispersion accelerates it.

Comparison between the 3D and 2D results show that the 2D results are qualitatively similar to the 3D results on all accounts, except when it comes to the impact of the Rayleigh number on the finger number density at the top boundary of the domain. In particular, the results on the impact of the dispersion parameters S and α on the dynamics of convective dissolution are qualitatively similar in 2D and 3D.

This work thus provides a systematic assessment of the impact of hydrodynamic dispersion on convective dissolution in the context of the subsurface storage of CO_2 . In doing so it also explains the discrepancy between the previous numerical and experimental studies of the impact of dispersion on the efficiency of convective dissolution. It opens prospects towards a precise mapping of the onset time's behavior as a function of the dispersion parameters and over a wide range of Rayleigh number values. Experimental studies in which the dispersivity lengths are varied independently of the Rayleigh number would be very useful to provide a closer comparison to our findings, as would experiments where the dispersivity ratio can be adjusted (it is possible by various means, see^{47,48}). Note that recent pore scale experiments suggest that Darcy scale simulations

Accepted to *Phys. Fluids* 10.1063/5.0086370

Convective dissolution of Carbon Dioxide in porous media: impact of dispersion

may not be able to grasp the full complexity of the coupling between pore scale convection and solute transport¹⁰; further developments may require incorporating pore-scale effects under the purview of continuum-scale modelling in order to properly model the convection finger velocity in porous media without sacrificing the essential low-cost computational advantage provided by continuum simulations.

ACKNOWLEDGMENTS

This work was supported by ANR (Agence Nationale de la Recherche – the French National Research Agency) under project *CO₂-3D* (grant nr. ANR-16-CE06-0001) and by Région Bretagne under project *CO₂seq3D* (grant nr. SAD17049). We acknowledge enlightening discussions with J. Carrera Ramírez and J. J. Hidalgo during the course of the project. We also thank C. Soulaïne and N. Mukherjee for suggestions regarding the numerical setup of the OpenFOAM model.

Appendix A: Impact of the 2D grid size on the temporal evolution of the solute flux

The impact of the grid size on the predicted convective dissolution was tested prior to the parametric study. In Fig. 17 we show the evolution of the solute flux obtained in the two-dimensional geometry for $Ra = 3000$, $S = 20$; $\alpha = 0.1$, and for three different grid sizes: 400×400 , 1000×1000 , and 1500×1500 . The plots obtained for the two largest grid sizes are absolutely identical for $0 \leq \tilde{t} \leq 1$; in particular, the nonlinear onset time is not impacted by the linear grid size as long as the latter is as large as 1000, which is the value chosen for our parametric study. The time evolution of the mean concentration (or, equivalently, total dissolved mass of CO₂), also display very close behaviors (not shown here) between the two grid sizes until asymptotic times.

The log-log scale shows the $t^{-1/2}$ scaling expected at short times (diffusive regime, see the end of section II F).

Appendix B: Validation of the numerical model

To validate the numerical model, we have run our OpenFOAM simulation with the parameters considered by Tilton, Daniel, and Riaz⁶, and confronted our predicted temporal evolution to that predicted by the numerical simulation of these authors, which used a spectral discretization

Convective dissolution of Carbon Dioxide in porous media: impact of dispersion

method. As shown in Fig. 18 where the dimensionless flux, \bar{J} , is plotted as a function of the dimensionless time, \bar{t} , the agreement between the two predictions is excellent over the entire time range ($0 < \bar{t} \leq 10$). Note that $Ra = 500$ and that the dispersion parameters (S and α) was set to 0 in our simulation, as Tilton, Daniel, and Riaz⁶ did not consider hydrodynamic dispersion.

Appendix C: Spatial distributions of horizontal and vertical components of the velocity

The maps of the components of velocity \tilde{u}_x and \tilde{u}_y in the two-dimensional geometry addressed in Fig. 2, show that the horizontal velocities are largest at the top boundary of the domain, where the vertical velocity component is necessarily zero, and emphasize the finger structure in the \tilde{u}_y maps.

Appendix D: Impact of the dispersivity ratio on the penetration depth and finger number density

Fig. 20 shows that for $Ra = 3000$ the value of the dispersivity ratio α , investigated at 0.1, 0.3 and 0.5, does not significantly impact the time evolution of the finger penetration depth nor the vertical profiles of the finger number density (FND). The penetration depth averages (on average over time) with α , but marginally, whereas for the FND no trend is visible.

Appendix E: On non-dimensionalization strategies

Our findings on the role of hydrodynamic dispersion in convective dissolution are consistent with a number of previous experimental observations^{9,11,30}. The apparent contradiction between these findings and a number of previous numerical predictions^{14,28} can be explained by the non-dimensionalization scheme used in these studies (as well as in Ref.²⁹). They consider the same non-dimensional governing equations as used in the present study, namely Eq. (5) (in the case of¹⁴ they are slightly different as rock matrix compressibility is taken into account), but they non-dimensionalize the dispersion tensor in the following manner:

$$\bar{\mathbf{D}} = (1 - S' + S'\alpha\|\mathbf{u}\|)\mathbf{I} + S'(1 - \alpha)\frac{\bar{u}_i\bar{u}_j}{\|\mathbf{u}\|}, \quad (\text{E1})$$

where α is the dispersivity ratio as defined in the present study, and $S' = (\alpha_L u^*)(D_0 + \alpha_L u^*)$ is the longitudinal dispersion strength, which takes values in the range $[0, 1]$. This equation can be

Convective dissolution of Carbon Dioxide in porous media: impact of dispersion

TABLE II. Values of the physical parameters for the simulation illustrated in Fig. 21.

Physical parameter	Parameter value
Medium permeability (κ)	10^{-10} m^2
Medium porosity (ϕ)	0.3
Viscosity (η)	0.001 Pa·s
Diffusion coefficient (D_0)	$10^{-9} \text{ m}^2/\text{s}$
Density difference ($\Delta\rho$)	10 kg/m ³
Longitudinal dispersivity length (α_L)	$2.25 \cdot 10^{-2} \text{ m}$ ($S = 20$) and $2.8 \cdot 10^{-4} \text{ m}$ (for $S = 0.25$)
Ratio of dispersivity lengths (α)	0.1
Channel height (H)	1 m
Channel length (L)	3 m
Initial concentration at top (c_0)	1 arb. unit

compared to Eq. (7) in our non-dimensionalization scheme, where the $1 - S'$ term in the factor of \mathbf{I} in Eq. E1 above is replaced by 1, and the longitudinal dispersion strength $S = (\alpha_L u^*)/D_0$ takes values in the range $[0; +\infty]$. Obviously the two parameters accounting for the dispersion's strength are related to each other through $S = S'/(1 - S')$ or $S' = S/(1 + S)$. Consequently, when using Eq. (E1) together with Eq. (5) to describe the coupled flow and solute transport dynamics, the Rayleigh number Ra' which Ghesmat, Hassanzadeh, and Abedi²⁸ define must be $Ra(1 - S') = Ra/(1 + S)$, since the dimensional equations which they considered are identical to Eq. (2). In other words, Ra' is defined using an effective diffusion coefficient $D_0 + \alpha_L u^*$. Hence the dispersion strength S' (or, equivalently, S) cannot be varied independently of the Rayleigh number Ra' : with any increase in dispersion strength, Ra' decreases. On the contrary, the Rayleigh number Ra (the one we use) is independent of S' or S .

To illustrate its effect we show in Fig. 21 how increasing the longitudinal dispersion strength impacts the convective fingers in a simulation that is based on our non-dimensionalized equations (5) and (7) (Fig. 21a and 21b), and in a simulation based on the non-dimensionalization scheme defined by Eq. (5) and (E1) (Fig. 21c and 21d). Fig. 21a shows the concentration field obtained at non-dimensional time $\tilde{t} = 5$ for a dimensional configuration defined by the dimensional parameters of Table II; the Rayleigh number is $Ra = 3000$, the longitudinal dispersion strength $S = 0.25$, and the dispersivity ratio $\alpha = 0.1$. Fig. 21b shows the same concentration field for the same

Convective dissolution of Carbon Dioxide in porous media: impact of dispersion

configuration as in Fig. 21b, except that the longitudinal dispersion strength is now $S = 20$. As discussed at length in section III, the solute fingers are thicker and penetrate more slowly into the flow domain when $S = 20$ than when $S = 0.2$ (compare Fig. 21b to 21a). Fig. 12 was obtained with the same domain size, medium properties and fluid properties as in Fig. 21a, but using the second non-dimensionalization scheme with $Ra' = 2400$, $S' = 0.2$, and $\alpha = 0.1$; in terms of our non-dimensional parameters, this corresponds to $Ra = 3000$, $S = 0.25$, and $\alpha = 0.1$, i.e., to the exact same dimensional system as that of Fig. 21a; hence the concentration field is exactly identical to that in the latter subfigure. Fig. 21d was obtained with the same parameters as Fig. 21c, except that the longitudinal dispersion strength was increased to $S' = 0.95$ (corresponding to $S = 20$ as in Fig. 21b). We see that with this non-dimensionalization scheme the finger have become much more narrow and have penetrated farther into the flow domain when increasing the dispersion strength; the reason is that, while Ra' has been kept constant between Fig. 21c and Fig. 21d), the effective Rayleigh number Ra has changed and is equal to 48000 in Fig. 21d, a much larger value for which the convection is much stronger. Conversely, for Fig. 21d to display the same concentration field as Fig. 21b, Ra' would have to be set to 142.86.

This explains why Hidalgo and Carrera¹⁴ and Ghesmat, Hassanzadeh, and Abedi²⁸ have observed a very strong decrease of the nonlinear onset time as a function of the dispersion strength: increasing S' strongly increases the effective Rayleigh number Ra , which speeds up the onset of convection very much.

REFERENCES

- ¹I. panel on climate change (IPCC), “Climate change 2013: The physical science basis. fifth assessment report,” Tech. Rep. (IPCC Secretariat, Geneva, Switzerland, 2013).
- ²D. Daniel, N. Tilton, and A. Riaz, “Optimal perturbations of gravitationally unstable, transient boundary layers in porous media,” *J. Fluid Mech.* **727**, 456–487 (2013).
- ³H. E. Huppert and J. A. Neufeld, “The fluid mechanics of carbon dioxide sequestration,” *Annu. Rev. Fluid Mech.* **46**, 255–272 (2014).
- ⁴N. Tilton and A. Riaz, “Nonlinear stability of gravitationally unstable, transient, diffusive boundary layers in porous media,” *J. Fluid Mech.* **745**, 251–278 (2014).
- ⁵A. Riaz, M. Hesse, H. Tchelepi, and F. Orr, “Onset of convection in a gravitationally unstable diffusive boundary layer in porous media,” *J. Fluid Mech.* **548**, 87–111 (2006).

Convective dissolution of Carbon Dioxide in porous media: impact of dispersion

- ⁶N. Tilton, D. Daniel, and A. Riaz, “The initial transient period of gravitationally unstable diffusive boundary layers developing in porous media,” *Phys. Fluids* **25**, 092107 (2013).
- ⁷H. Emami-Meybodi, H. Hassanzadeh, C. P. Green, and J. Ennis-King, “Convective dissolution of CO₂ in saline aquifers: Progress in modeling and experiments,” *Int. J. Greenh. Gas Con.* **40**, 238–266 (2015).
- ⁸A. Vreme, F. Nadal, B. Pouligny, P. Jeandet, G. Liger-Belair, and P. Meunier, “Gravitational instability due to the dissolution of carbon dioxide in a Hele-Shaw cell,” *Phys. Rev. Fluids* **1**, 064301 (2016).
- ⁹Y. Liang, B. Wen, M. A. Hesse, and D. DiCarlo, “Effect of dispersion on solutal convection in porous media,” *Geophys. Res. Lett.* **45**, 9690–9698 (2018).
- ¹⁰C. Brouzet, Y. Méheust, F. Nadal, and P. Meunier, “CO₂ convective dissolution in a 3-D granular porous medium: an experimental study,” *Phys. Rev. Fluids* (2021), submitted.
- ¹¹L. Wang, Y. Nakanishi, A. Hyodo, and T. Suekane, “Three-dimensional structure of natural convection in a porous medium: Effect of dispersion on finger structure,” *Int. J. Greenh. Gas Con.* **53**, 274–283 (2016).
- ¹²R. Liyanage, J. Cen, S. Krevor, J. P. Crawshaw, and R. Pini, “Multidimensional observations of dissolution-driven convection in simple porous media using x-ray CT scanning,” *Transport Porous Med.* **126**, 355–378 (2019).
- ¹³P. Cheng, M. Besthorn, and A. Firoozabadi, “Effect of permeability anisotropy on buoyancy-driven flow for CO₂ sequestration in saline aquifers,” *Water Resour. Res.* **48**, 2012WR011939 (2012).
- ¹⁴J. J. Hidalgo and J. Carrera, “Effect of dispersion on the onset of convection during CO₂ sequestration,” *J. Fluid Mech.* **640**, 441–452 (2009).
- ¹⁵J. A. Neufeld, M. A. Hesse, A. Riaz, M. A. Hallworth, H. A. Tchelepi, and H. E. Huppert, “Convective dissolution of carbon dioxide in saline aquifers,” *Geophys. Res. Lett.* **37** (2010).
- ¹⁶M. T. Elenius and K. Johannsen, “On the time scales of nonlinear instability in miscible displacement porous media flow,” *Computat. Geosci.* **16**, 901–911 (2012).
- ¹⁷G. S. Pau, J. B. Bell, K. Pruess, A. S. Almgren, M. J. Lijewski, and K. Zhang, “High-resolution simulation and characterization of density-driven flow in CO₂ storage in saline aquifers,” *Adv. Water Res.* **3**, 443–455 (2010).
- ¹⁸D. R. Hewitt, J. A. Neufeld, and J. R. Lister, “High Rayleigh number convection in a three-dimensional porous medium,” *J. Fluid Mech.* **748**, 879–895 (2014).

Convective dissolution of Carbon Dioxide in porous media: impact of dispersion

- ¹⁹X. Fu, L. Cueto-Felgueroso, and R. Juanes, “Pattern formation and coarsening dynamics in three-dimensional convective mixing in porous media,” *Philos. T. Roy. Soc. A* **371**, 20120355 (2013).
- ²⁰C. Green and J. Ennis-King, “Steady flux regime during convective mixing in three-dimensional heterogeneous porous media,” *Fluids* **3**, 58 (2018).
- ²¹S. Pirozzoli, M. De Paoli, F. Zonta, and A. Soldati, “Towards the ultimate regime in Rayleigh–Darcy convection,” *Journal of Fluid Mechanics* **911** (2021).
- ²²J. Fried and M. Combarous, “Dispersion in porous media,” (Elsevier, 1971) pp. 169–282.
- ²³T. Perkins, O. Johnston, *et al.*, “A review of diffusion and dispersion in porous media,” *Soc. Petrol. Eng. J.* **3**, 70–84 (1963).
- ²⁴B. Bijeljic and M. J. Blunt, “Pore-scale modeling of transverse dispersion in porous media,” *Water Resour. Res.* **43**, 1–8 (2007).
- ²⁵H. Erfani, M. Babaei, and V. Niasar, “Dynamics of CO₂ density-driven flow in carbonate aquifers: Effects of dispersion and geochemistry,” *Water Resour. Res.* **57**, 1–26 (2021).
- ²⁶B. Wen, K. W. Chang, and M. A. Hesse, “Rayleigh-darcy convection with hydrodynamic dispersion,” *Phys. Rev. Fluids* **3**, 123801 (2018).
- ²⁷M. De Paoli, “Influence of reservoir properties on the dynamics of a migrating current of carbon dioxide,” *Phys. Fluids* **33**, 016602 (2021).
- ²⁸K. Ghesmat, H. Hassanzadeh, and J. Abedi, “The effect of anisotropic dispersion on the convective mixing in long-term CO₂ storage in saline aquifers,” *AIChE J.* **57**, 561–570 (2011).
- ²⁹H. Emami-Meybodi, “Dispersion-driven instability of mixed convective flow in porous media,” *Phys. Fluids* **29**, 094102 (2017).
- ³⁰T. Menand and A. Woods, “Dispersion, scale, and time dependence of mixing zones under gravitationally stable and unstable displacements in porous media,” *Water Resour. Res.* **41**, 1–13 (2005).
- ³¹Y. Xie, C. T. Simmons, and A. D. Werner, “Speed of free convective fingering in porous media,” *Water Resour. Res.* **47**, 1–16 (2011).
- ³²R. A. Schincariol, F. W. Schwartz, and C. A. Mendoza, “On the generation of instabilities in variable density flow,” *Water Resour. Res.* **30**, 913–927 (1994).
- ³³N. Tilton, “Onset of transient natural convection in porous media due to porosity perturbations,” *J. Fluid Mech.* **838**, 129–147 (2018).
- ³⁴A. Selim and D. A. S. Rees, “The stability of a developing thermal front in a porous medium. i

Convective dissolution of Carbon Dioxide in porous media: impact of dispersion

- linear theory," *J. Porous Media* **10**, 1–16 (2007).
- ³⁵H. Liu and J. Dane, "A numerical study on gravitational instabilities of dense aqueous phase plumes in three-dimensional porous media," *J. Hydrol.* **194**, 126–142 (1997).
- ³⁶J. P. Ennis-King and L. Paterson, "Role of convective mixing in the long-term storage of carbon dioxide in deep saline formations," *SPE J.* **10**, 349–356 (2005).
- ³⁷K. Ghesmat, H. Hassanzadeh, and J. Abedi, "The impact of geochemistry on convective mixing in a gravitationally unstable diffusive boundary layer in porous media: CO₂ storage in saline aquifers," *J. Fluid Mech.* **673**, 480–512 (2011).
- ³⁸A. C. Slim, "Solutal-convection regimes in a two-dimensional porous medium," *J. Fluid Mech.* **741**, 461–491 (2014).
- ³⁹R. L. Davis, J. E. Carter, and M. Hafez, "Three-dimensional viscous flow solutions with a vorticity-stream function formulation," *AIAA J.* **27**, 892–900 (1989).
- ⁴⁰R. F. Warming and R. M. Beam, "Upwind second-order difference schemes and applications in aerodynamic flows," *AIAA J.* **14**, 1241–1249 (1976).
- ⁴¹T. Le Borgne, M. Dentz, D. Bolster, J. Carrera, J.-R. De Dreuzy, and P. Davy, "Non-fickian mixing: Temporal evolution of the scalar dissipation rate in heterogeneous porous media," *Advances in Water Resources* **33**, 1468–1475 (2010).
- ⁴²N. B. Engdahl, T. R. Ginn, and G. E. Fogg, "Scalar dissipation rates in non-conservative transport systems," *J. Contam. Hydrol.* **149**, 46–60 (2013).
- ⁴³J. J. Hidalgo, J. Fe, L. Cueto-Felgueroso, and R. Juanes, "Scaling of convective mixing in porous media," *Physical review letters* **109**, 264503 (2012).
- ⁴⁴J. Fernandez, P. Kurowski, P. Petitjeans, and E. Meiburg, "Density-driven unstable flows of miscible fluids in a hele-shaw cell," *J. Fluid Mech.* **451**, 239–260 (2002).
- ⁴⁵Y. Nakanishi, A. Hyodo, L. Wang, and T. Suekane, "Experimental study of 3d rayleigh–taylor convection between miscible fluids in a porous medium," *Adv. Water Res.* **97**, 224–232 (2016).
- ⁴⁶P. C. Carman, "Permeability of saturated sands, soils and clays," *J. Agr. Sci.* **29**, 262–273 (1939).
- ⁴⁷J. D. C. Jacob, R. Krishnamoorti, and C. J. C., "Particle dispersion in porous media: Differentiating effects of geometry and fluid rheology," *Phys. Rev. E* **96**, 022610 (2017).
- ⁴⁸Y. Yang, T. Liu, Y. Li, Y. Li, Z. You, M. Zuo, P. Diwu, R. Wang, X. Zhang, and J. Liang, "Effects of velocity and permeability on tracer dispersion in porous media," *Appl. Sci.* **11**, 4411 (2021).

This is the author's peer reviewed, accepted manuscript. However, the online version of record will be different from this version once it has been copyedited and typeset.

PLEASE CITE THIS ARTICLE AS DOI: 10.1063/5.0086370

Accepted to Phys. Fluids 10.1063/5.0086370

Convective dissolution of Carbon Dioxide in porous media: impact of dispersion

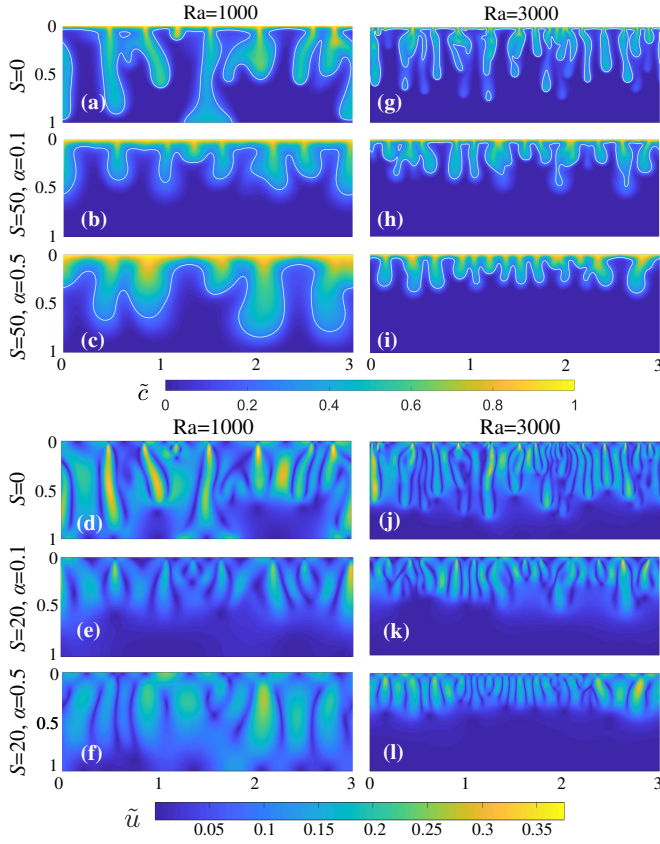


FIG. 2. Comparison of concentration (top panel) and velocity (bottom panel) fields in the 2D geometry. In each panel the left column (a-f) shows the data at dimensionless time $\tilde{t} = 10$ for $Ra = 1000$, while the right column (g-l) shows the data at dimensionless time $\tilde{t} = 6$ for $Ra = 3000$. The first line of subfigures in each panel (a, d, g, j) corresponds to no hydrodynamic dispersion ($S = 0$), the second one (b, e, h, k) to a strong but significantly anisotropic hydrodynamic dispersion ($S = 50$, $\alpha = 0.1$), and the third one (c, f, i, l) to a strong but less anisotropic dispersion ($S = 50$, $\alpha = 0.5$). The white line superimposed to the concentration maps is the iso- \tilde{c} line at $\tilde{c} = 0.25$.

This is the author's peer reviewed, accepted manuscript. However, the online version of record will be different from this version once it has been copyedited and typeset.

PLEASE CITE THIS ARTICLE AS DOI: 10.1063/5.0086370

Accepted to Phys. Fluids 10.1063/5.0086370

Convective dissolution of Carbon Dioxide in porous media: impact of dispersion

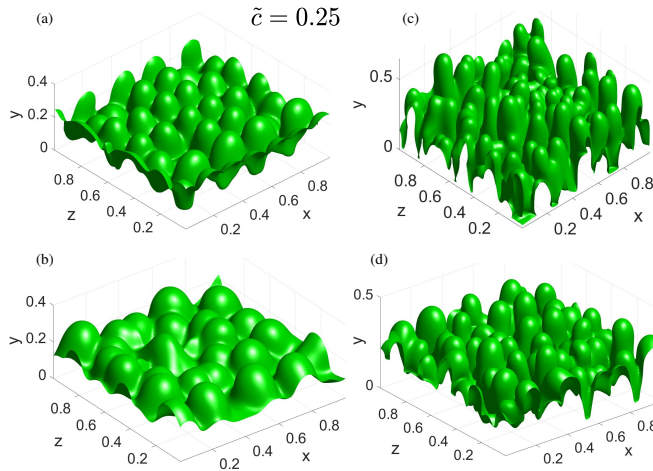


FIG. 3. Comparison of inverted 3D finger patterns (i.e., iso- \bar{c} surfaces at $\bar{c} = 0.25$) at dimensionless time $\bar{t} = 4$, for $Ra = 1000$ (left column) and $Ra = 3000$ (right column), under different dispersion configurations: (a, c) $S = 0$ and (b, d) $S = 20$ with $\alpha = 0.1$.

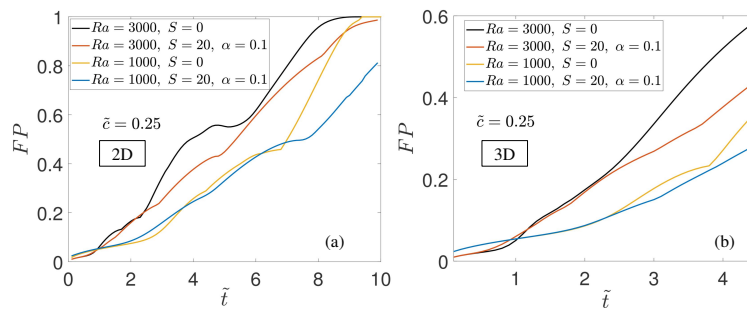


FIG. 4. Temporal evolution of the finger penetration depth (estimated as the mean altitude of the $\bar{c} = 0.25$ iso-line/surface) in the 2D (a) and 3D (b) geometries, for two Rayleigh numbers ($Ra = 1000$ and $Ra = 3000$) and two dispersion configuration (no dispersion and $S = 20$, $\alpha = 0.1$).

This is the author's peer reviewed, accepted manuscript. However, the online version of record will be different from this version once it has been copyedited and typeset.

PLEASE CITE THIS ARTICLE AS DOI: 10.1063/5.0086370

Accepted to Phys. Fluids 10.1063/5.0086370

Convective dissolution of Carbon Dioxide in porous media: impact of dispersion

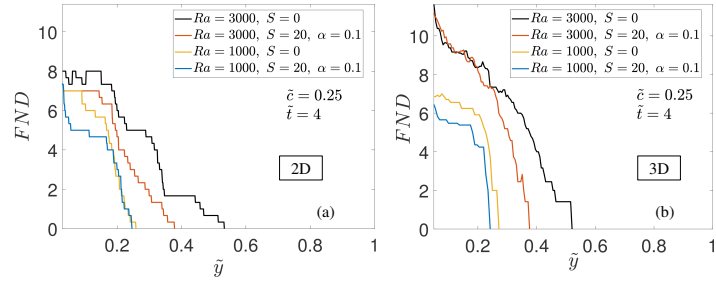


FIG. 5. Vertical profile of the finger number density in the 2D (a) and 3D (b) geometries, for two Rayleigh numbers ($Ra = 1000$ and $Ra = 3000$) and two dispersion configurations (no dispersion and $S = 20$, $\alpha = 0.1$), at time $\tilde{t} = 4$.

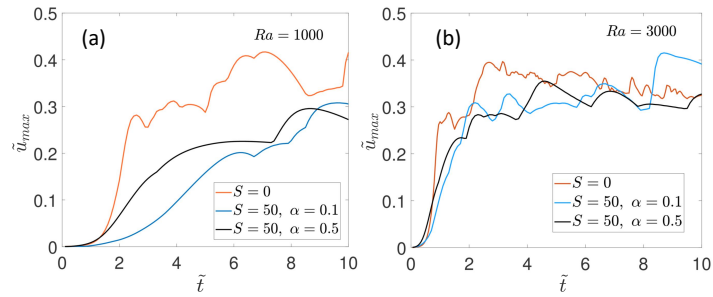


FIG. 6. Temporal evolution of the maximum flow velocity in the 2D domain for the dispersion configurations addressed in Fig. 2: (a) $Ra = 1000$ and (b) $Ra = 3000$.

This is the author's peer reviewed, accepted manuscript. However, the online version of record will be different from this version once it has been copyedited and typeset.

PLEASE CITE THIS ARTICLE AS DOI: 10.1063/5.0086370

Accepted to Phys. Fluids 10.1063/5.0086370

Convective dissolution of Carbon Dioxide in porous media: impact of dispersion

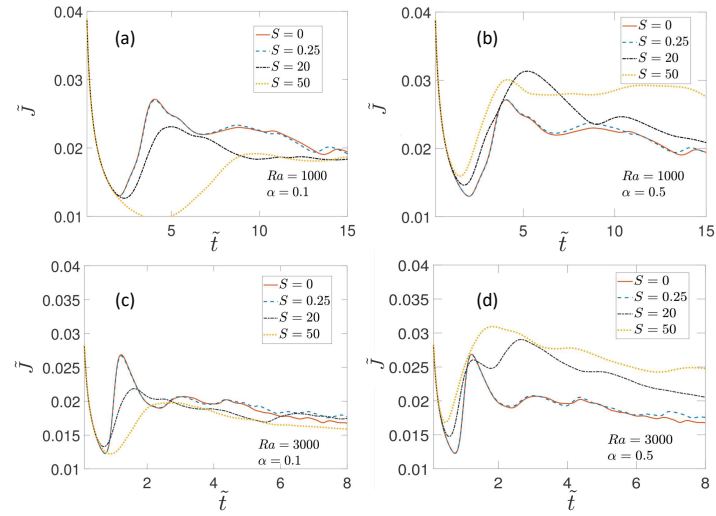


FIG. 7. Temporal evolution of the dispersive flux at the top boundary of the 2D flow domain for Rayleigh numbers $Ra = 1000$ – top line, i.e. (a, b) – and $Ra = 3000$ – bottom line, i.e. (c, d) – and for different values of the dispersive strength. The dispersivity ratio is $\alpha = 0.1$ – left column, i.e. (a, c) – or $\alpha = 0.5$ – right column, i.e. (b,d).

This is the author's peer reviewed, accepted manuscript. However, the online version of record will be different from this version once it has been copyedited and typeset.

PLEASE CITE THIS ARTICLE AS DOI: 10.1063/5.0086370

Accepted to Phys. Fluids 10.1063/5.0086370

Convective dissolution of Carbon Dioxide in porous media: impact of dispersion

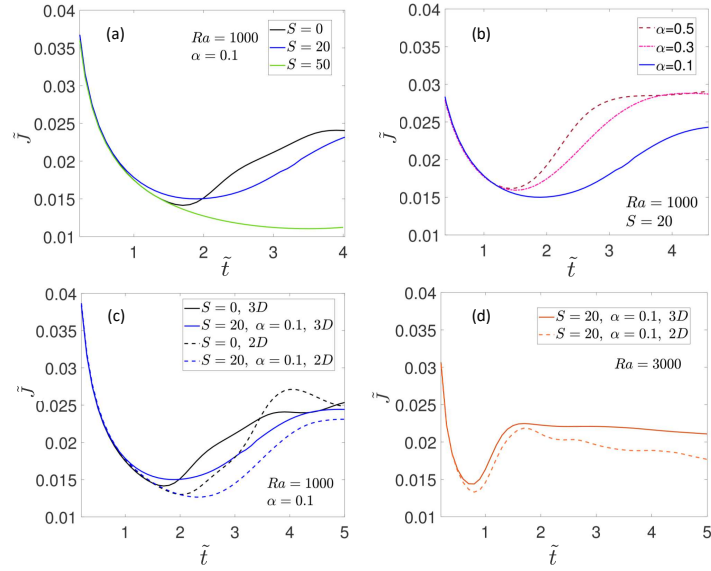


FIG. 8. (a,b): Temporal evolution of the dispersive flux at the top boundary of the 3D flow domain for Rayleigh number $Ra = 1000$: (a) for longitudinal dispersion strength $S = 20$ and different values of the dispersivity ratio, $\alpha = 0.1, 0.2$ and 0.3 ; (b) for dispersivity ratio $\alpha = 0.1$ and different longitudinal dispersion strengths $S = 0, 20$ and 50 . (c, d): Comparison between the results from the 2D and 3D simulations for $\alpha = 0.1$ and two longitudinal dispersion strengths $S = 0$ and 20 : (c) $Ra = 1000$ and (d) $Ra = 3000$.

This is the author's peer reviewed, accepted manuscript. However, the online version of record will be different from this version once it has been copyedited and typeset.

PLEASE CITE THIS ARTICLE AS DOI: 10.1063/5.0086370

Accepted to Phys. Fluids 10.1063/5.0086370

Convective dissolution of Carbon Dioxide in porous media: impact of dispersion

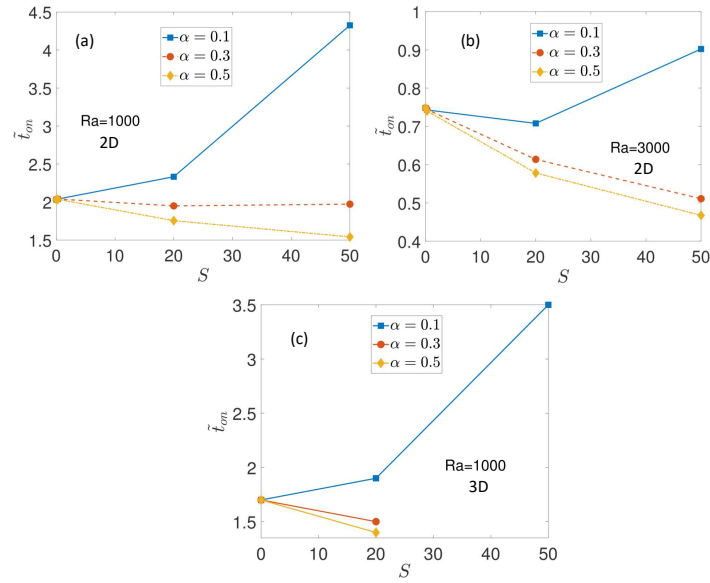


FIG. 9. Dependence of onset time on longitudinal dispersion strength S for various values of the dispersivity ratio α (a) in the 2D geometry for (a) $Ra = 1000$ and (b) $Ra = 3000$, and (c) in the 3D geometry for $Ra = 1000$.

Accepted to Phys. Fluids 10.1063/5.0086370

Convective dissolution of Carbon Dioxide in porous media: impact of dispersion

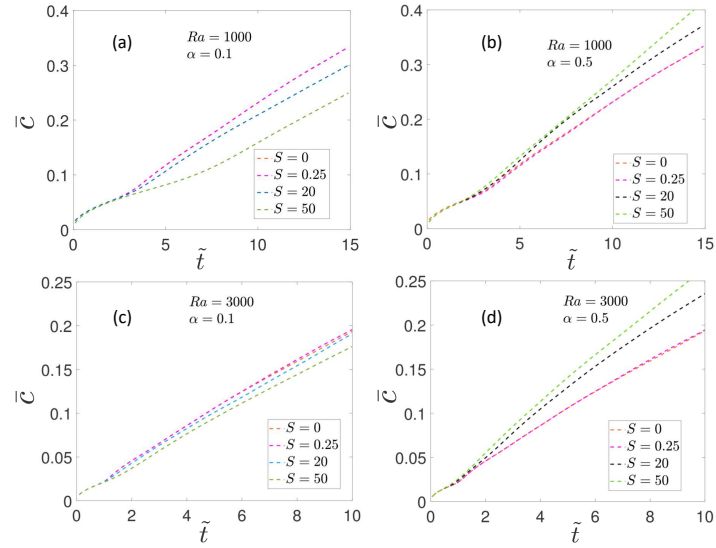


FIG. 10. Temporal evolution of the mean concentration in the entire flow domain for $Ra = 1000$ (a, b) and $Ra = 3000$ (c, d), and for $\alpha = 0.1$ (a, c) and $\alpha = 0.5$ (b, d).

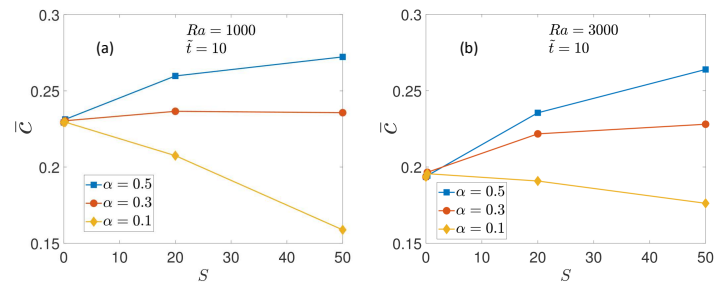


FIG. 11. Dependence of the mean concentration on the longitudinal dispersion strength S at dimensionless time $\tilde{t} = 10$ in the 2D geometry, for values of the dispersivity ratio α of 0.1, 0.3 and 0.5, and for (a) $Ra = 1000$ and (b) $Ra = 3000$.

Accepted to Phys. Fluids 10.1063/5.0086370

Convective dissolution of Carbon Dioxide in porous media: impact of dispersion

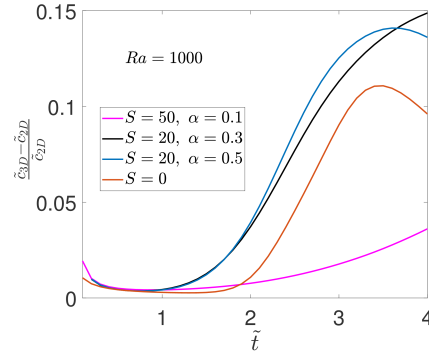


FIG. 12. Relative difference between the temporal evolution of the concentration in the 2D geometry and in the 3D geometry, for different longitudinal dispersion strengths and dispersivity ratios.

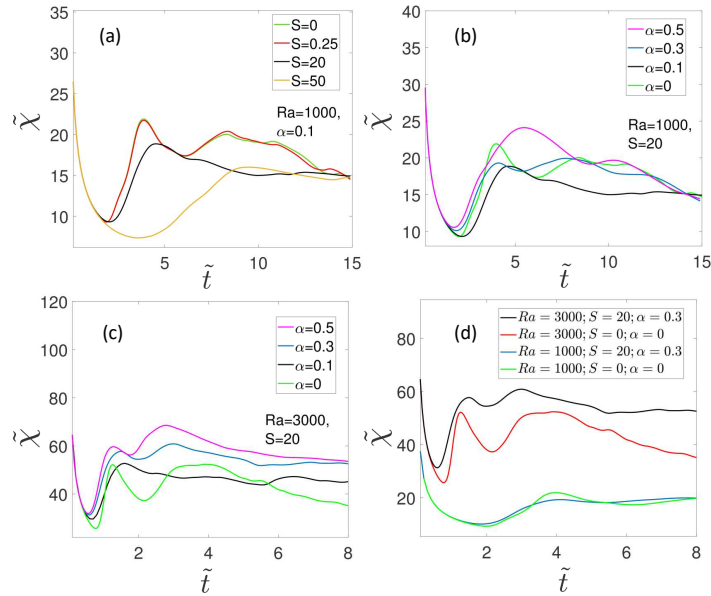


FIG. 13. Temporal evolution of the scalar dissipation rate in the 2D geometry a) for $Ra = 1000$ and for different longitudinal dispersion strengths S with $\alpha = 0.1$, and b) for $Ra = 1000$ and for different dispersivity ratios α with $S = 20$; c) is identical to b), except for the value of the Rayleigh number, which is $Ra = 3000$; d) shows a comparison between configurations which differ only by the Rayleigh number ($Ra = 1000$ or $Ra = 3000$).

Accepted to Phys. Fluids 10.1063/5.0086370

Convective dissolution of Carbon Dioxide in porous media: impact of dispersion

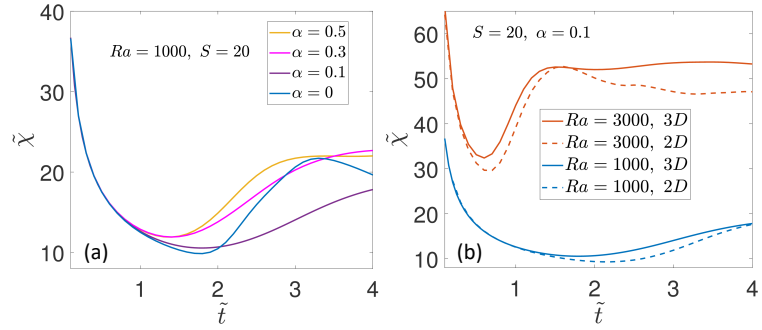


FIG. 14. (a) Same plot as that in Fig. 13b, but in the 3D geometry. (b) Comparison between results obtained in the 2D and 3D geometries for $S = 20$ and $\alpha = 0.1$, with either $Ra = 1000$ or $Ra = 3000$.

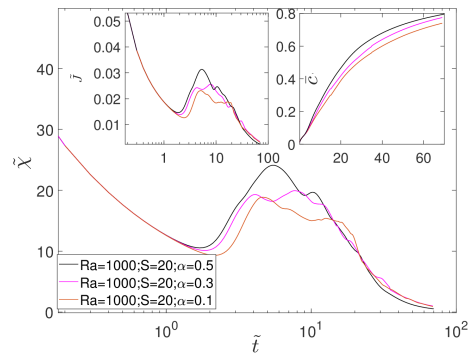


FIG. 15. Impact of the dispersivity ratio for $Ra = 1000$ and $S = 20$ on the scalar dissipation rate at large time, as well as on the total dissolution flux (left inset), and mean concentration (right inset).

This is the author's peer reviewed, accepted manuscript. However, the online version of record will be different from this version once it has been copyedited and typeset.

PLEASE CITE THIS ARTICLE AS DOI: 10.1063/5.0086370

Accepted to Phys. Fluids 10.1063/5.0086370

Convective dissolution of Carbon Dioxide in porous media: impact of dispersion

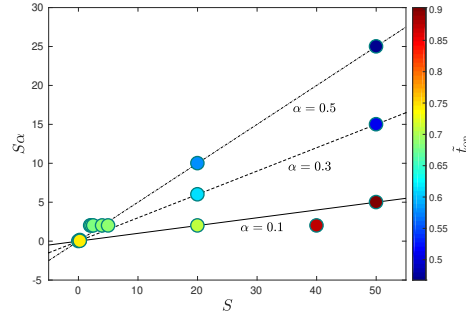


FIG. 16. Variations of the non-linear onset time in the $(S, S\alpha)$ space, which is a non-dimensional representation of the (D_L, D_T) space. Iso- α lines for $\alpha = 0.1, 0.2$ and 0.3 are shown as a solid, dashed and dot-dashed straight line, respectively.

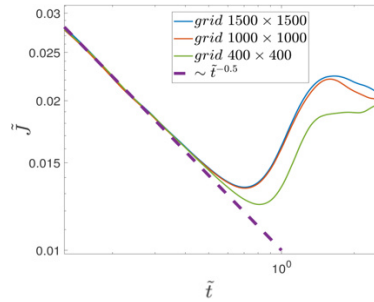


FIG. 17. Temporal evolution of the solute flux predicted by our model in the two-dimensional geometry for $Ra = 3000$, $S = 20$ and $\alpha = 0.1$, and for three grid sizes.

This is the author's peer reviewed, accepted manuscript. However, the online version of record will be different from this version once it has been copyedited and typeset.

PLEASE CITE THIS ARTICLE AS DOI: 10.1063/5.0086370

Accepted to *Phys. Fluids* 10.1063/5.0086370

Convective dissolution of Carbon Dioxide in porous media: impact of dispersion

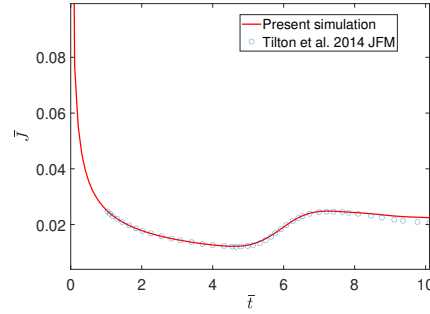


FIG. 18. Temporal evolution of the solute flux \bar{J} predicted by Tilton, Daniel, and Riaz⁶, and by our numerical simulation using the exact same parameters and no hydrodynamic dispersion.

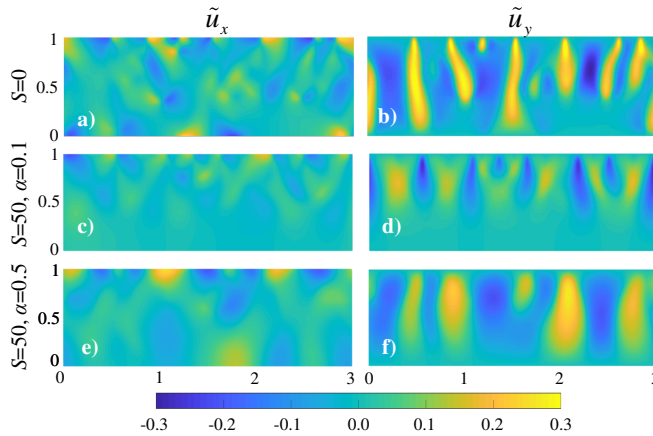


FIG. 19. Horizontal (a, c, e,) and vertical (b, d, f) components of the normalized 2D velocity field (\tilde{u}) corresponding to the left column of the bottom panel of Fig. 2, i.e., for $Ra = 1000$ and for three dispersion configurations indicated on the left of the velocity maps: $S = 0$ (a, b), $S = 50$ with $\alpha = 0.1$ (c, d), and $S = 50$ with $\alpha = 0.5$ (e, f).

This is the author's peer reviewed, accepted manuscript. However, the online version of record will be different from this version once it has been copyedited and typeset.

PLEASE CITE THIS ARTICLE AS DOI: 10.1063/5.0086370

Accepted to Phys. Fluids 10.1063/5.0086370

Convective dissolution of Carbon Dioxide in porous media: impact of dispersion

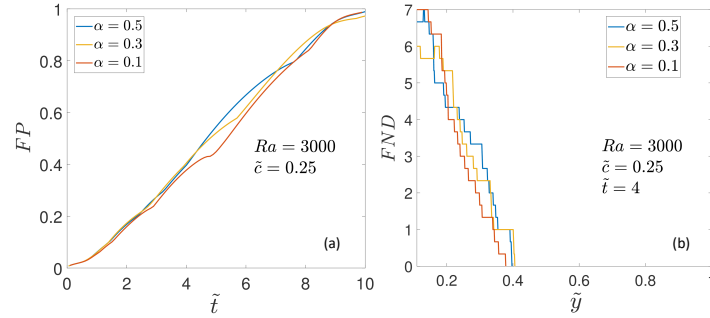


FIG. 20. (a) Time evolution of the finger penetration for $Ra = 3000$ and $S = 20$, and for three different values of the dispersivity ratio. (b) Vertical profiles of the finger number density at $\tilde{t} = 4$ for $Ra = 3000$, $S = 20$, and the same three α values.

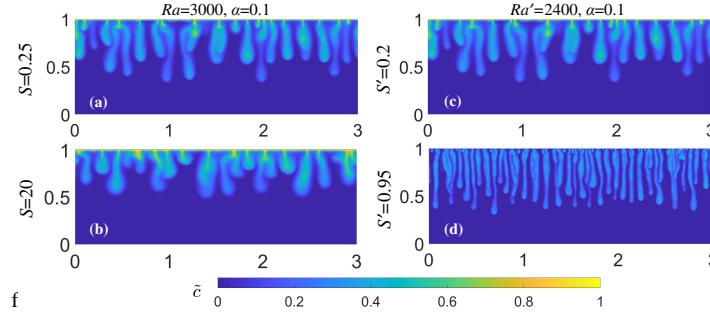
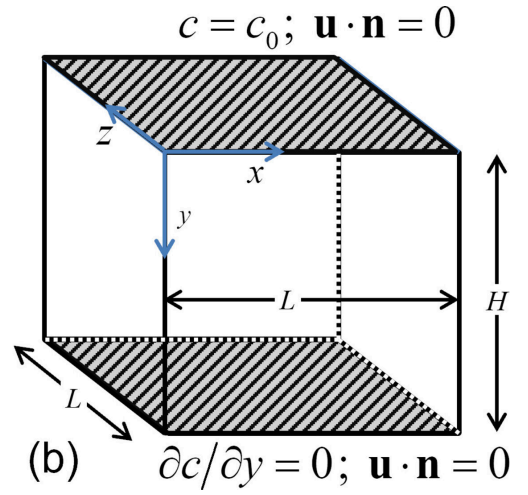
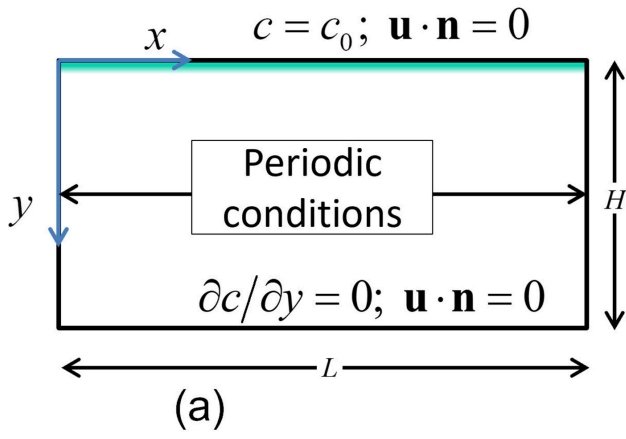


FIG. 21. (a, b): Snapshots of the concentration fields obtained at non-dimensional time $\tilde{t} = 5$ from the governing equations non-dimensionalized using our scheme (Eq. (5) and (7)), for a Rayleigh number $Ra = 3000$ and a dispersion tensor defined by $\alpha = 0.1$ and (a) $S = 0.25$ or (v) $S = 20$; the dimensional parameters are given in Table II. (c): Same as (a), but from governing equations non-dimensionalized using the scheme of Ghesmat, Hassanzadeh, and Abedi²⁸ (Eq. (5) and (E1)) for at Rayleigh number $Ra' = 2400$ and for a dispersion tensor defined by $\alpha = 0.1$ and $S' = 0.8$. (d) Same as (c), but for $S' = 0.95$.

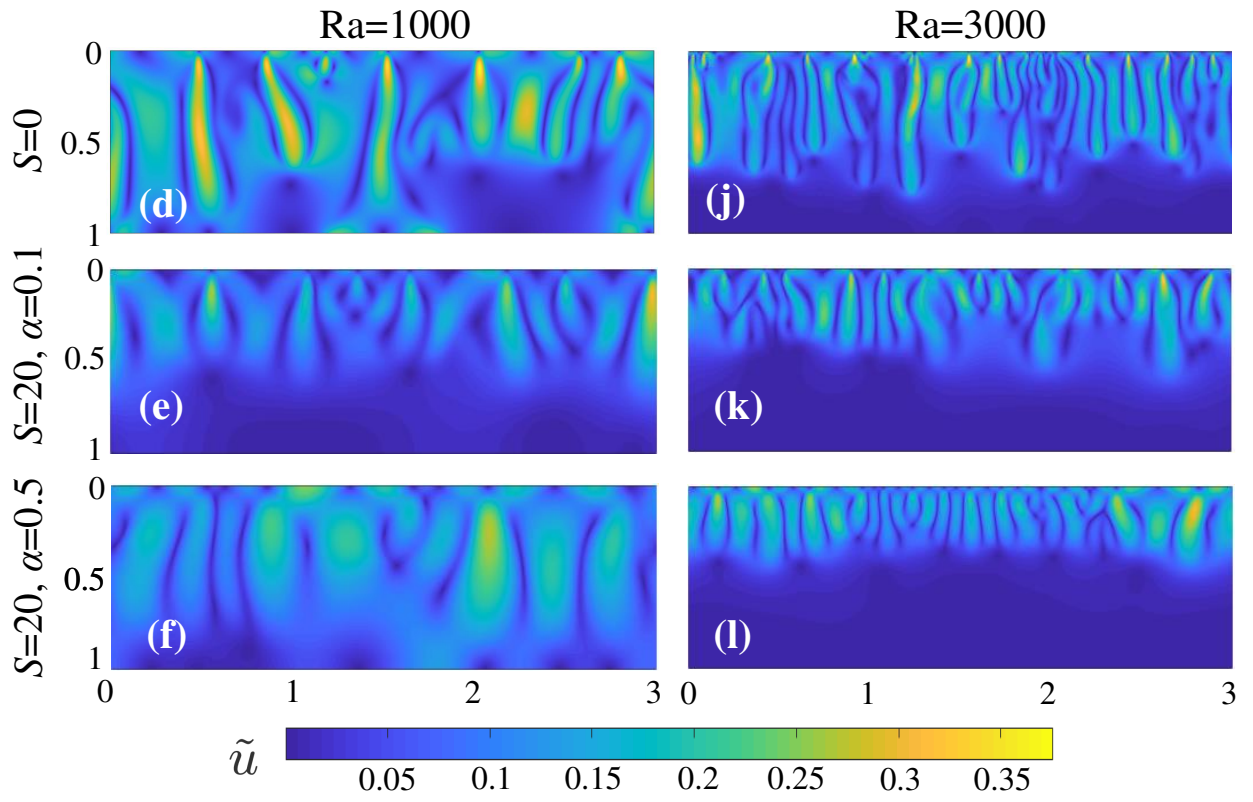
This is the author's peer reviewed, accepted manuscript. However, the online version of record will be different from this version once it has been copyedited and typeset.

PLEASE CITE THIS ARTICLE AS DOI: 10.1063/5.0086370



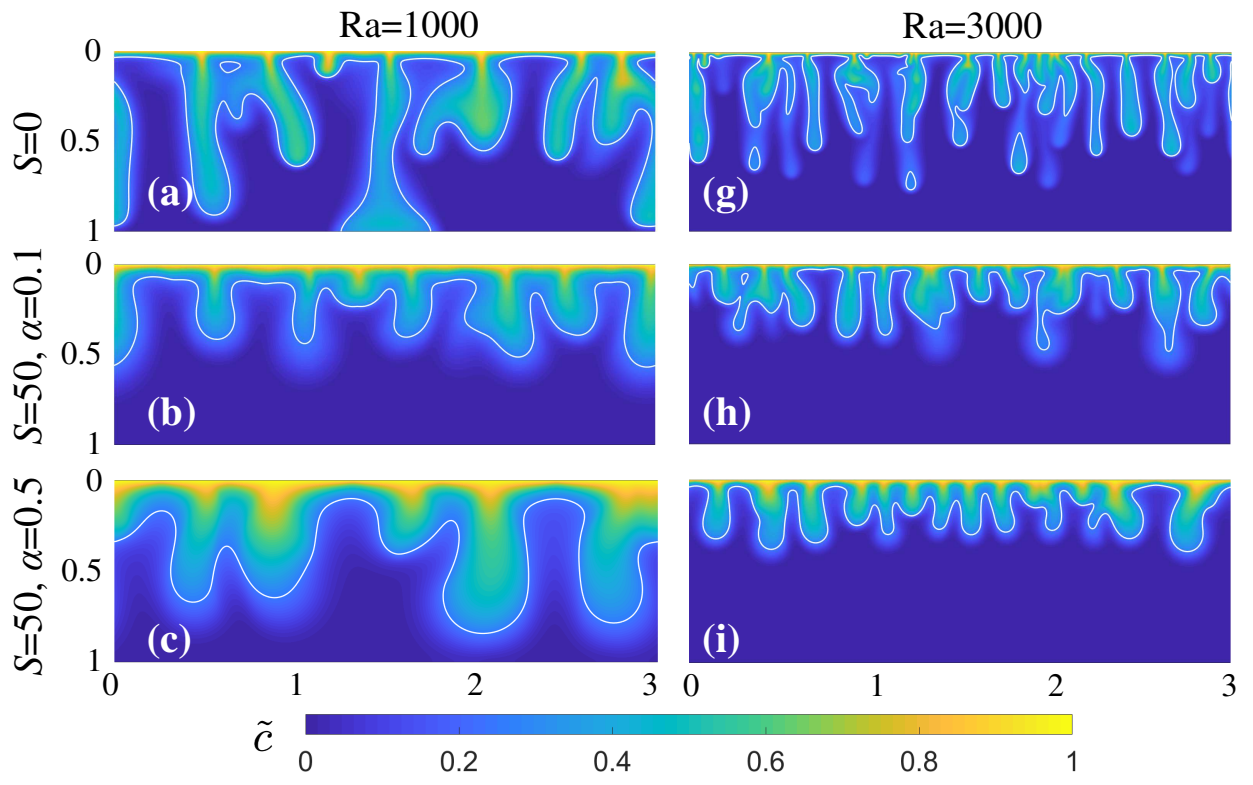
This is the author's peer reviewed, accepted manuscript. However, the online version of record will be different from this version once it has been copyedited and typeset.

PLEASE CITE THIS ARTICLE AS DOI: 10.1063/1.50086370



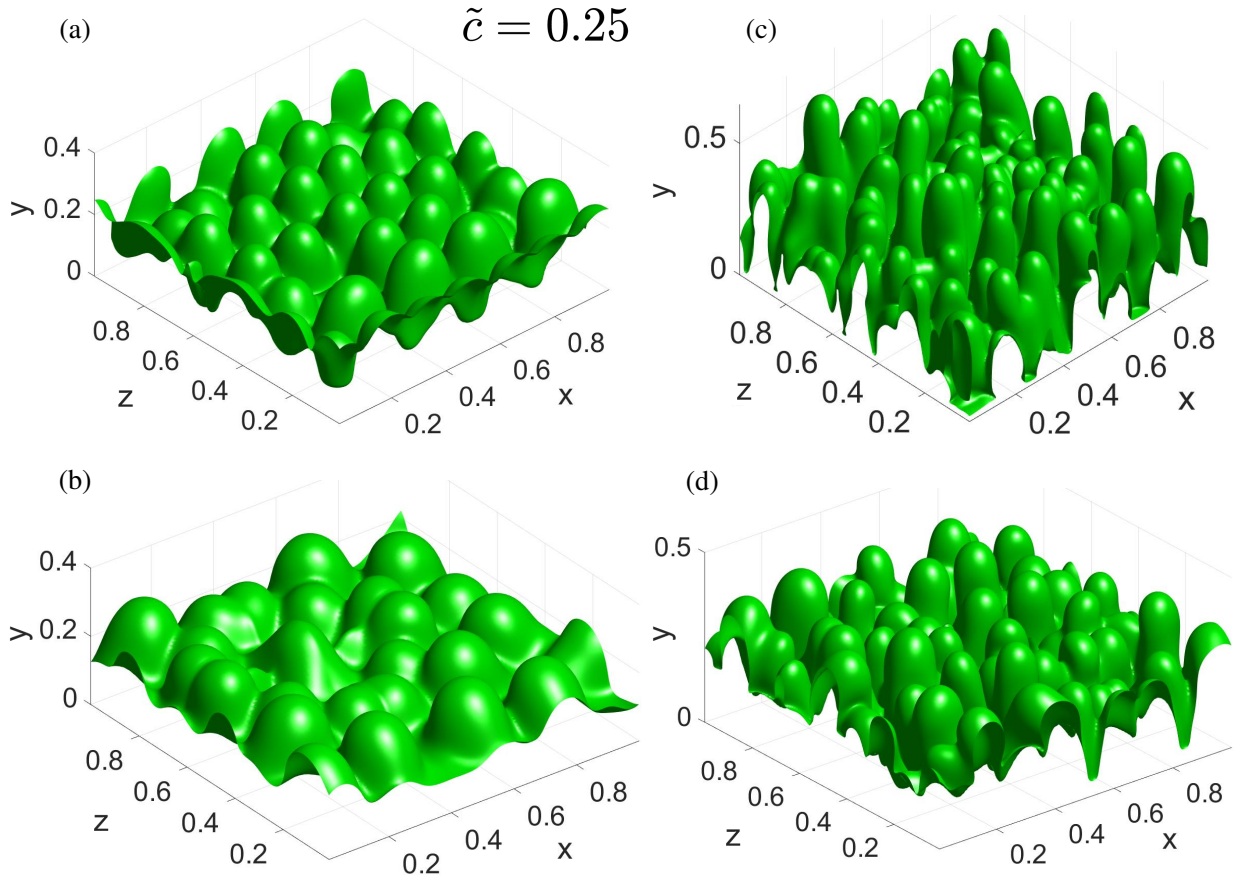
This is the author's peer reviewed, accepted manuscript. However, the online version of record will be different from this version once it has been copyedited and typeset.

PLEASE CITE THIS ARTICLE AS DOI: 10.1063/1.50086370



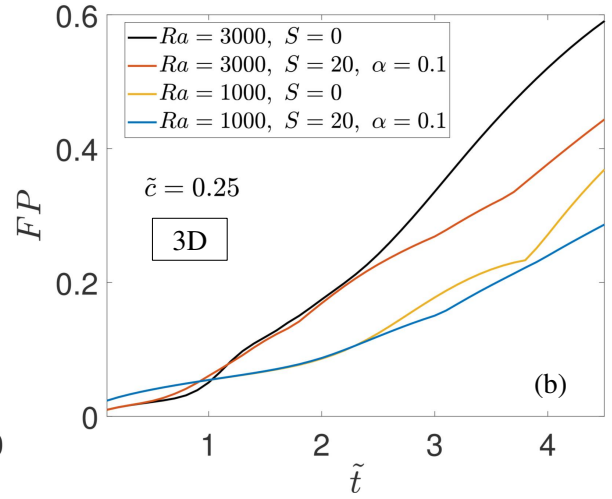
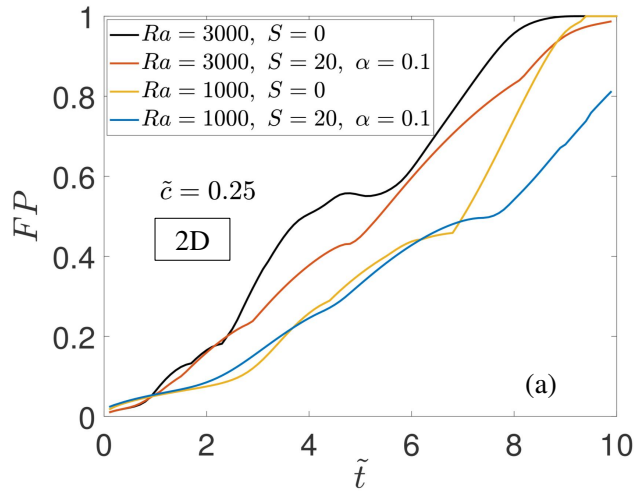
This is the author's peer reviewed, accepted manuscript. However, the online version of record will be different from this version once it has been copyedited and typeset.

PLEASE CITE THIS ARTICLE AS DOI: 10.1063/1.50086370



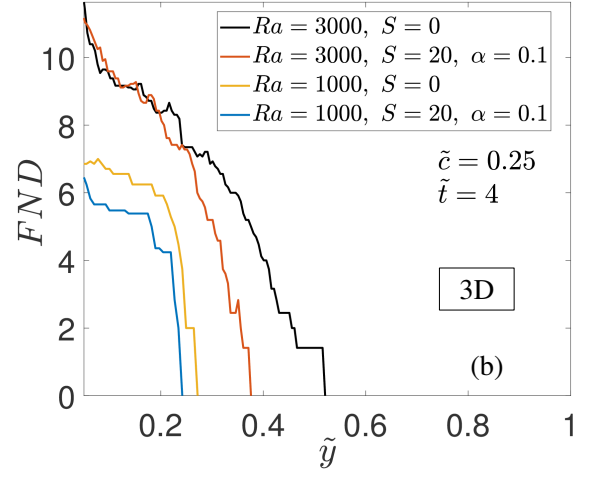
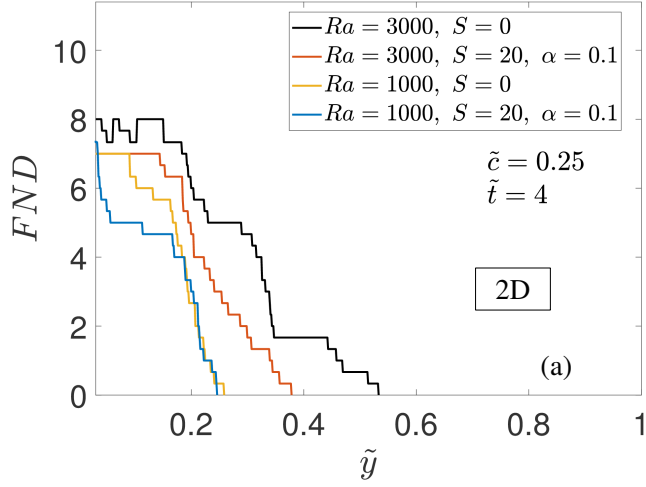
This is the author's peer reviewed, accepted manuscript. However, the online version of record will be different from this version once it has been copyedited and typeset.

PLEASE CITE THIS ARTICLE AS DOI: 10.1063/1.50086370



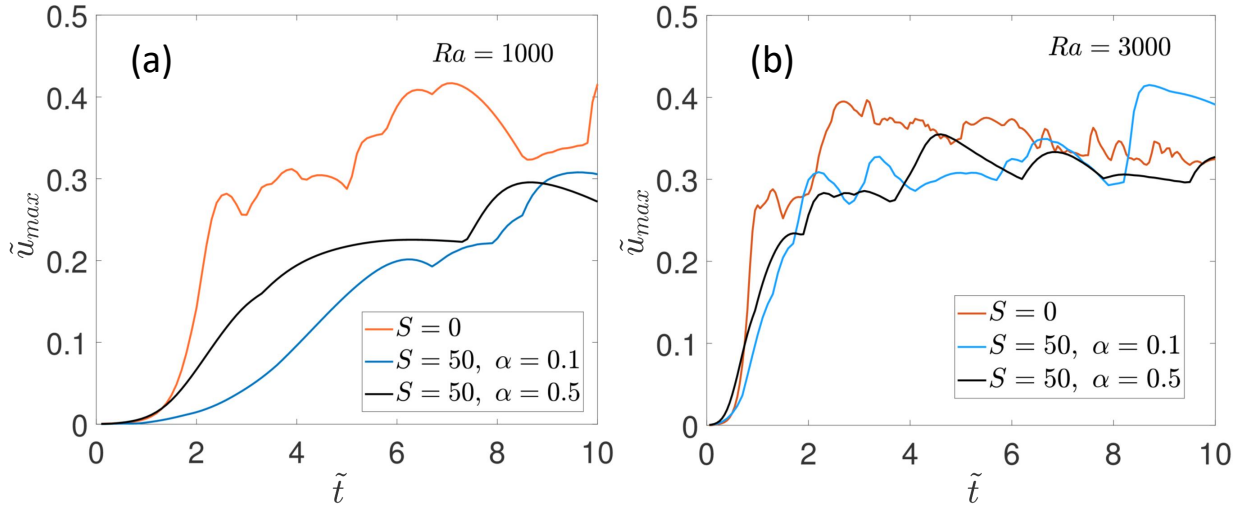
This is the author's peer reviewed, accepted manuscript. However, the online version of record will be different from this version once it has been copyedited and typeset.

PLEASE CITE THIS ARTICLE AS DOI: 10.1063/1.50086370



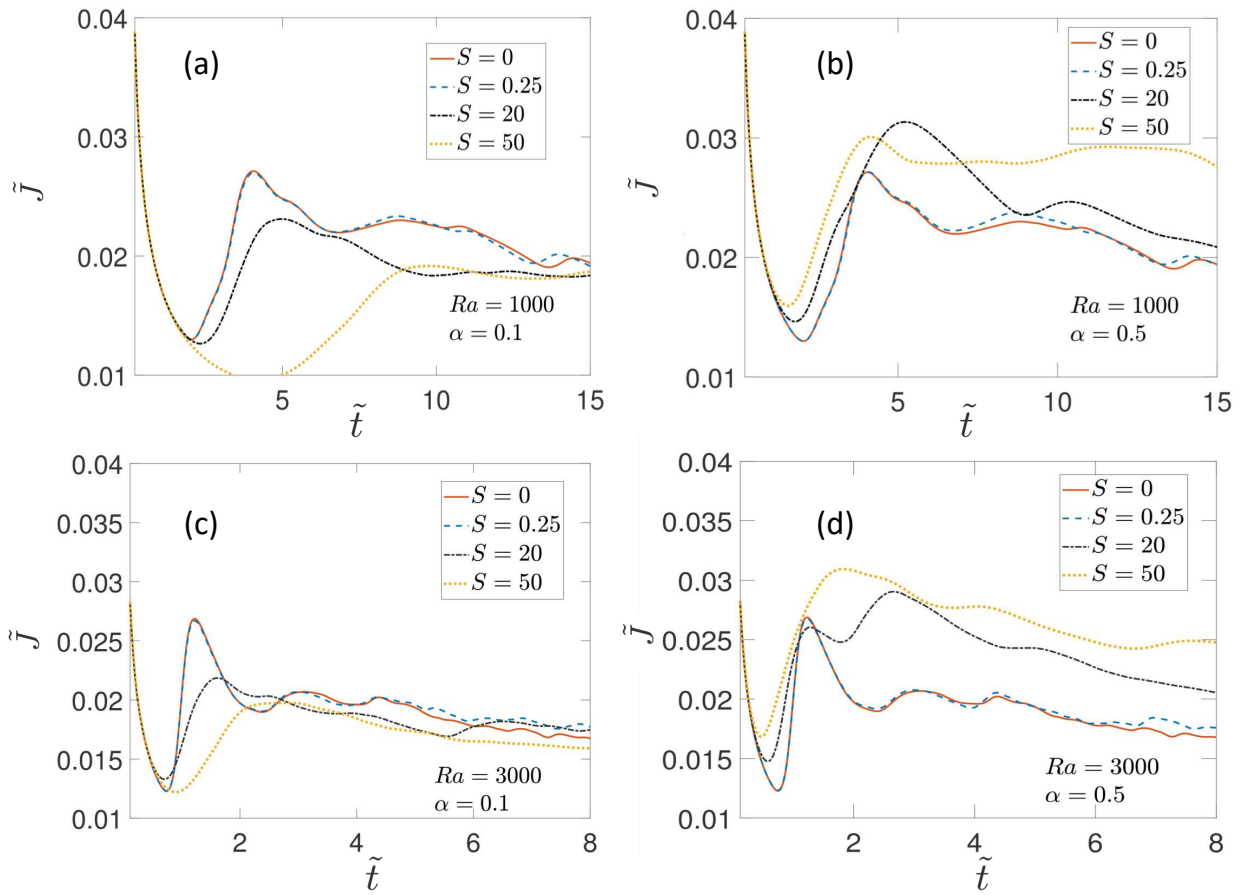
This is the author's peer reviewed, accepted manuscript. However, the online version of record will be different from this version once it has been copyedited and typeset.

PLEASE CITE THIS ARTICLE AS DOI: 10.1063/1.50086370



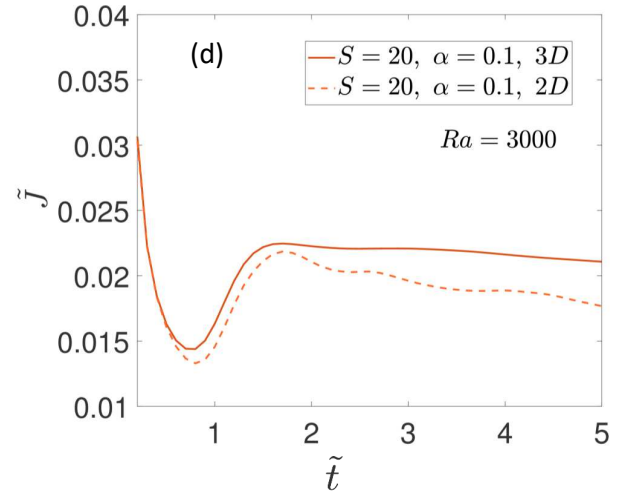
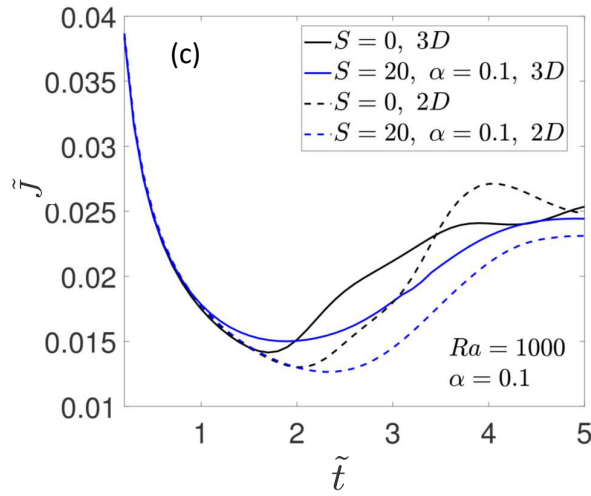
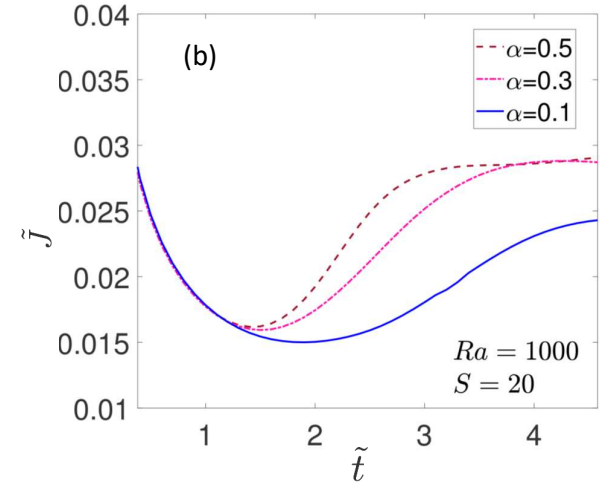
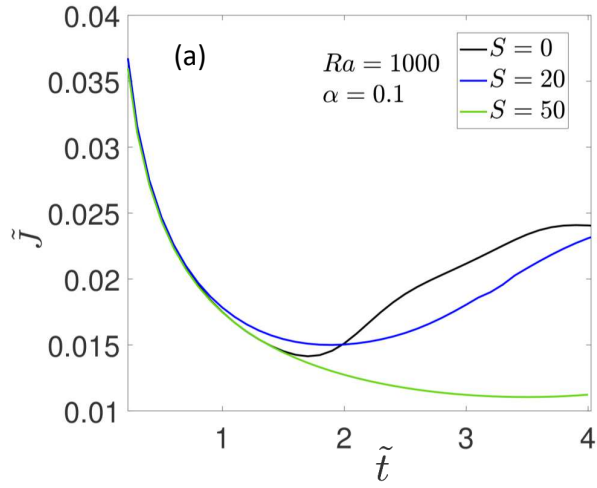
This is the author's peer reviewed, accepted manuscript. However, the online version of record will be different from this version once it has been copyedited and typeset.

PLEASE CITE THIS ARTICLE AS DOI: 10.1063/1.50086370



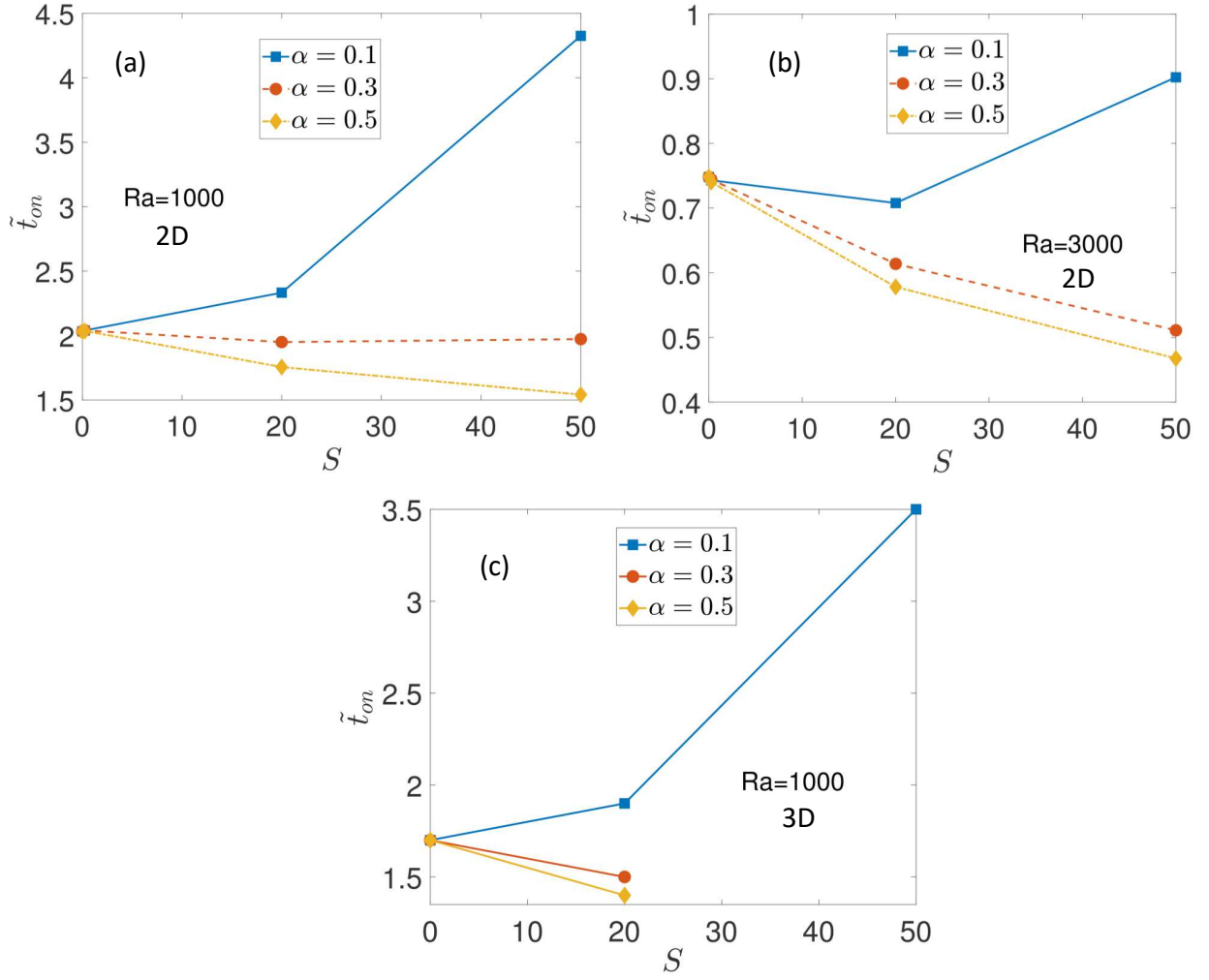
This is the author's peer reviewed, accepted manuscript. However, the online version of record will be different from this version once it has been copyedited and typeset.

PLEASE CITE THIS ARTICLE AS DOI: 10.1063/1.50086370



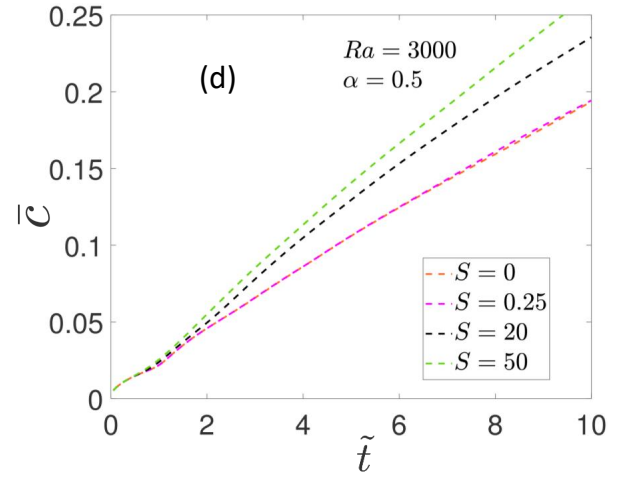
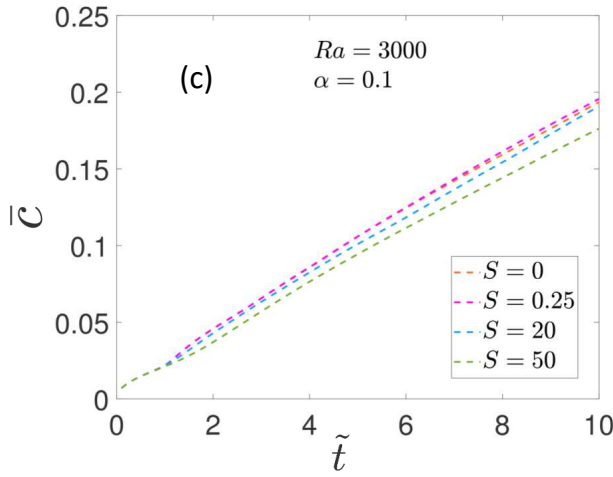
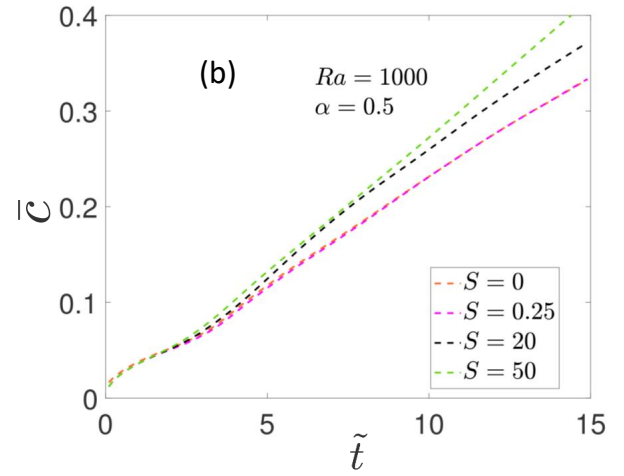
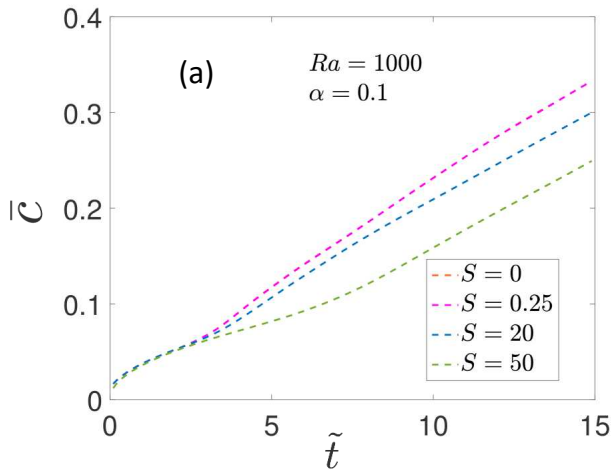
This is the author's peer reviewed, accepted manuscript. However, the online version of record will be different from this version once it has been copyedited and typeset.

PLEASE CITE THIS ARTICLE AS DOI: 10.1063/1.50086370



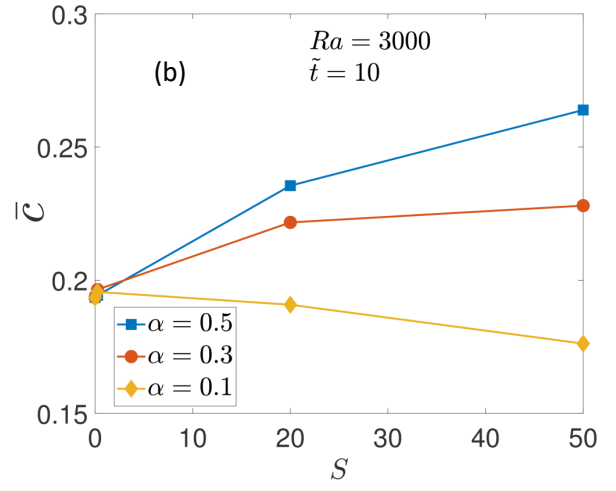
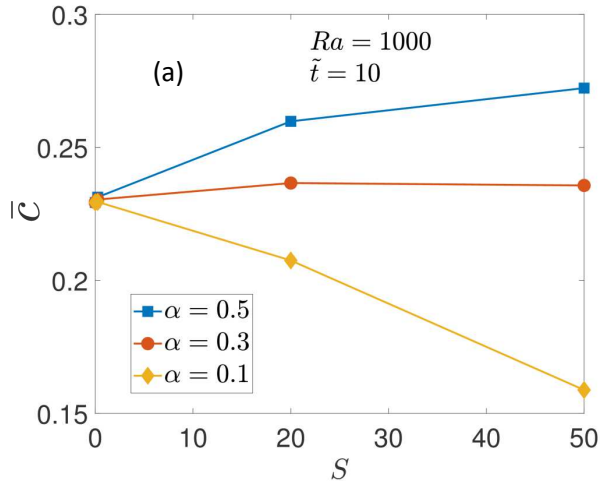
This is the author's peer reviewed, accepted manuscript. However, the online version of record will be different from this version once it has been copyedited and typeset.

PLEASE CITE THIS ARTICLE AS DOI: 10.1063/1.50086370



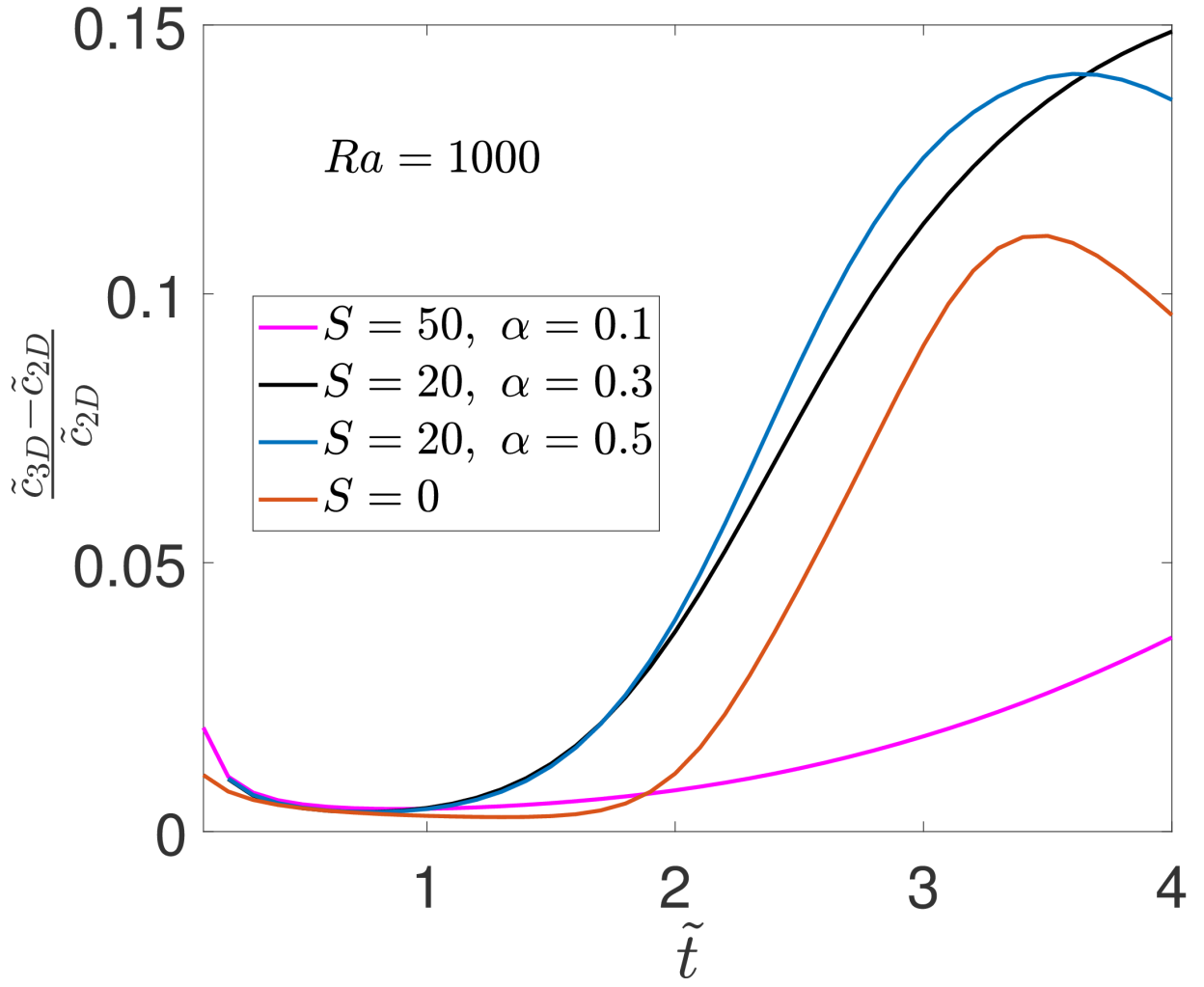
This is the author's peer reviewed, accepted manuscript. However, the online version of record will be different from this version once it has been copyedited and typeset.

PLEASE CITE THIS ARTICLE AS DOI: 10.1063/1.50086370



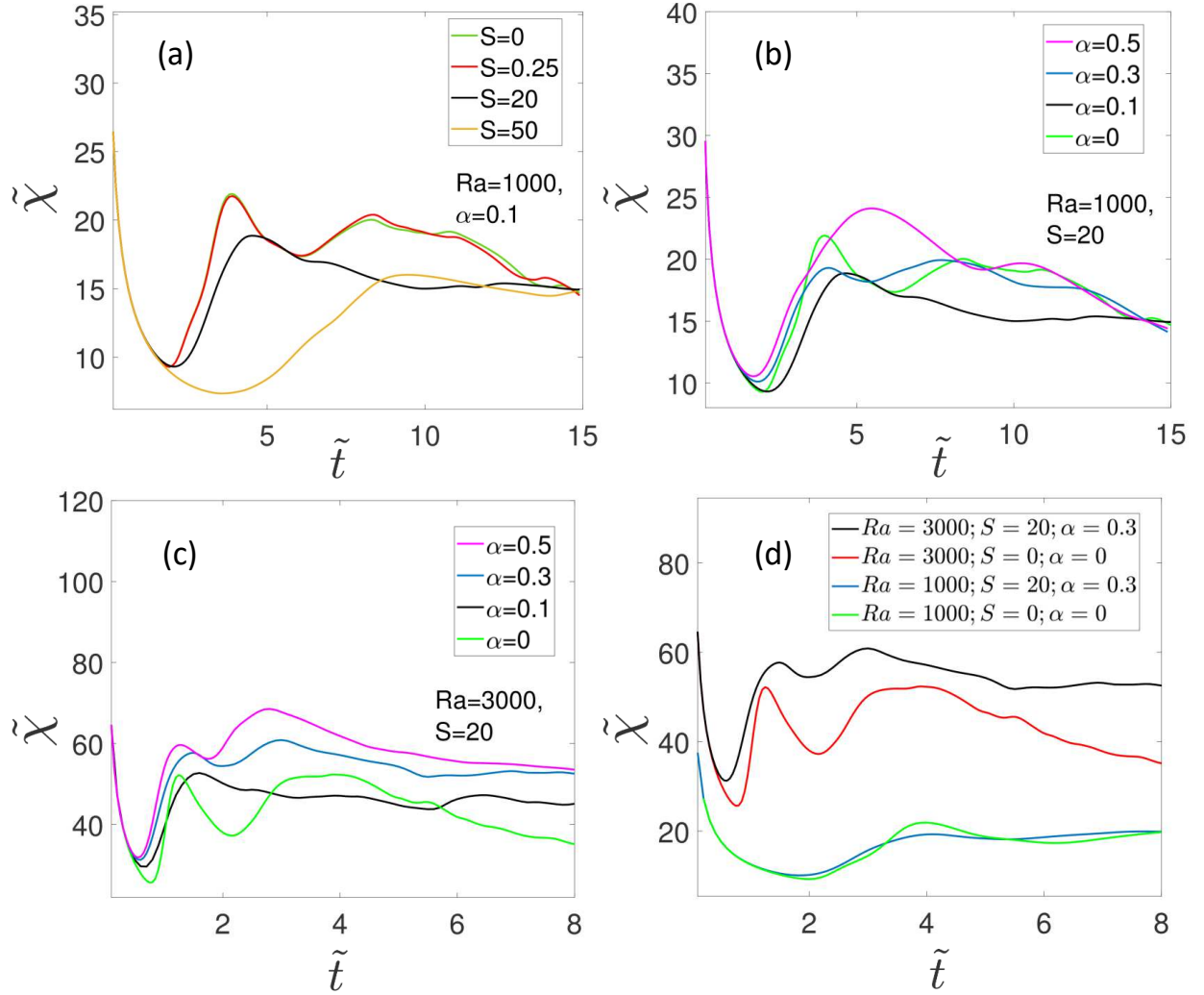
This is the author's peer reviewed, accepted manuscript. However, the online version of record will be different from this version once it has been copyedited and typeset.

PLEASE CITE THIS ARTICLE AS DOI: 10.1063/1.50086370



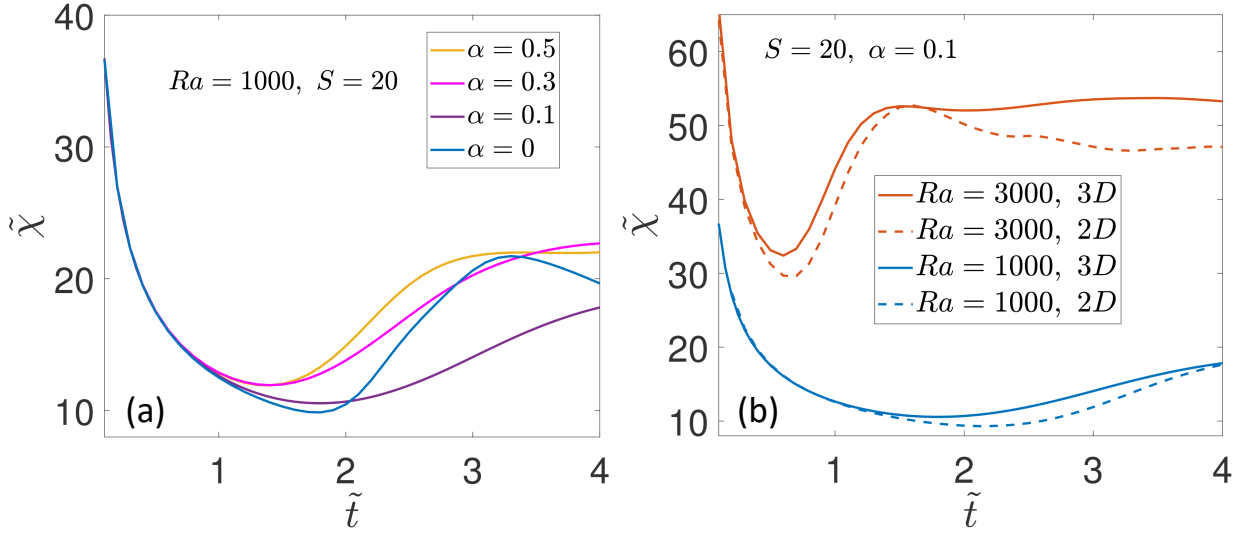
This is the author's peer reviewed, accepted manuscript. However, the online version of record will be different from this version once it has been copyedited and typeset.

PLEASE CITE THIS ARTICLE AS DOI: 10.1063/1.50086370



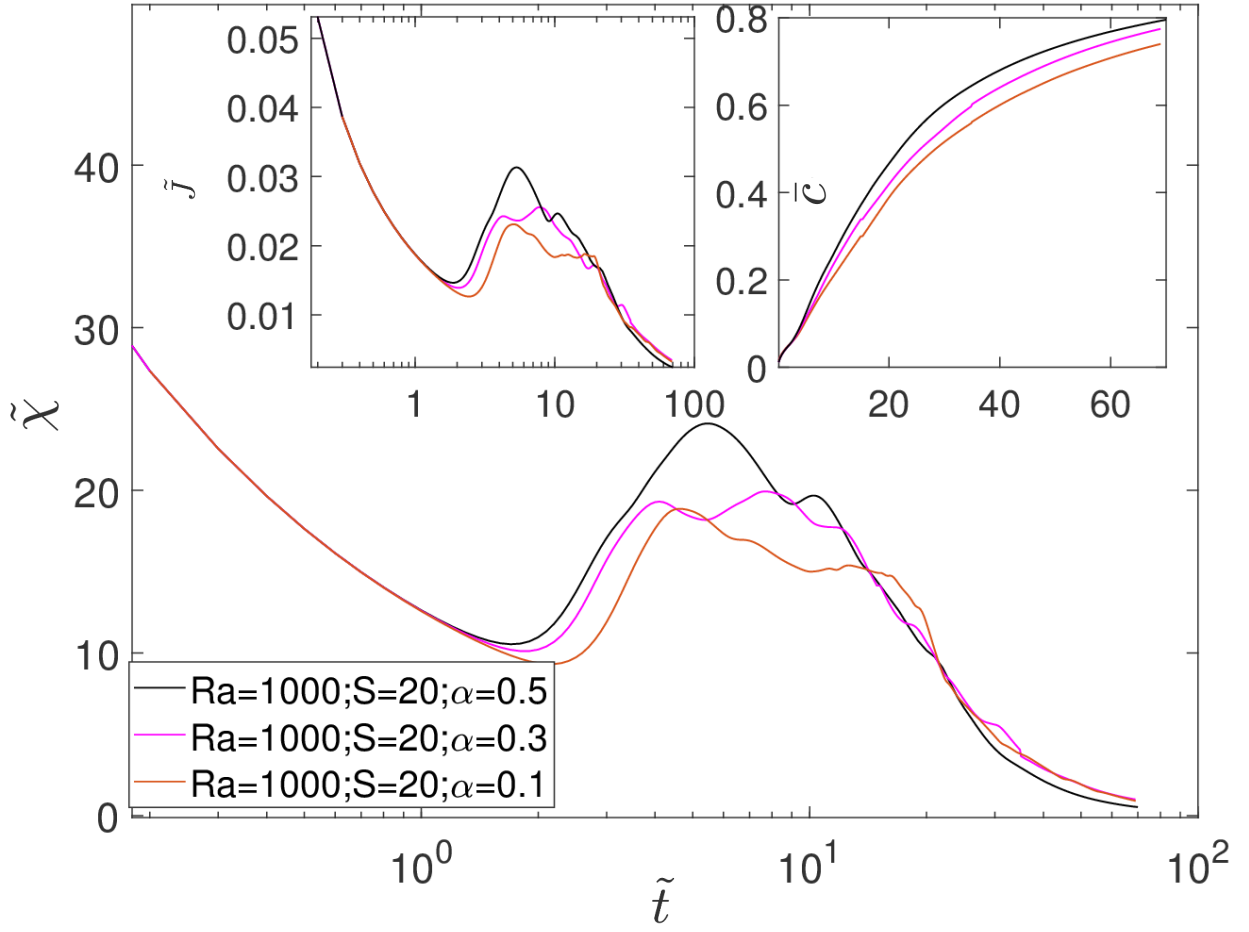
This is the author's peer reviewed, accepted manuscript. However, the online version of record will be different from this version once it has been copyedited and typeset.

PLEASE CITE THIS ARTICLE AS DOI: 10.1063/5.0086370



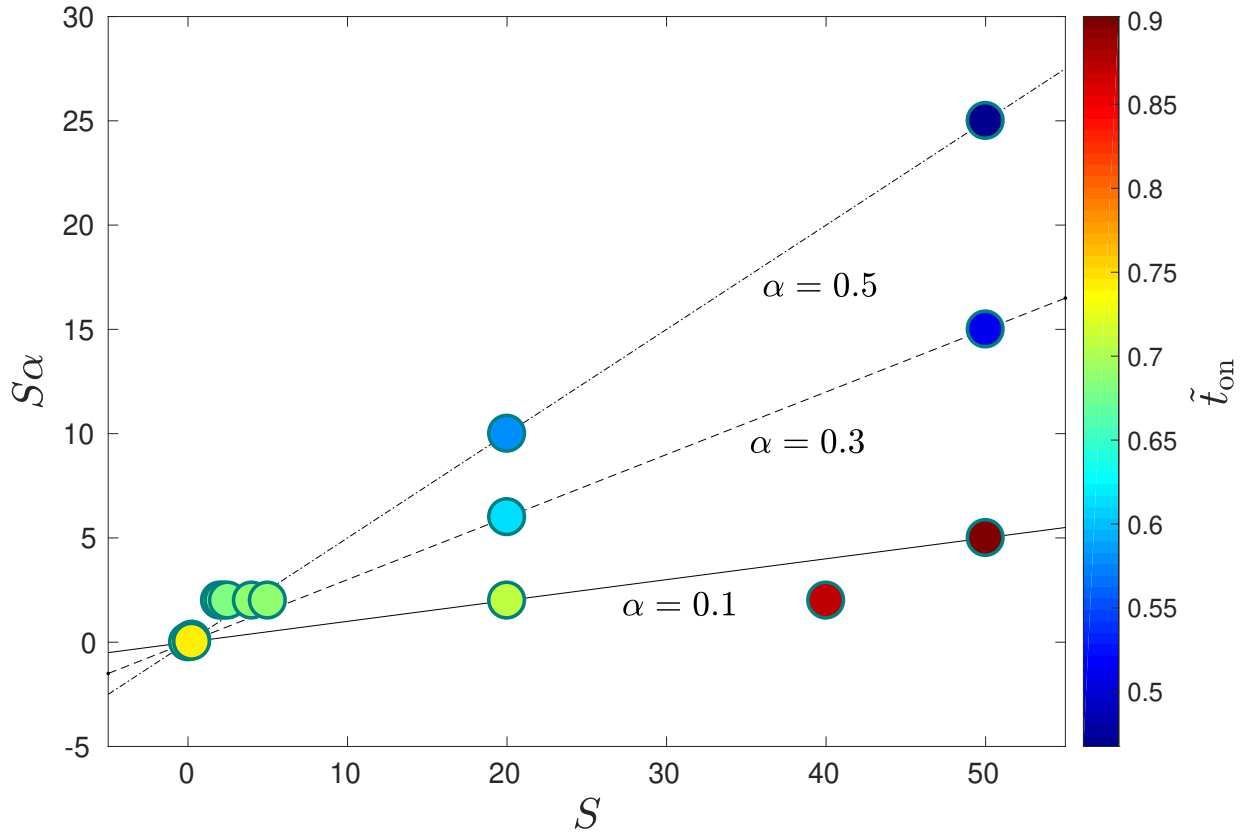
This is the author's peer reviewed, accepted manuscript. However, the online version of record will be different from this version once it has been copyedited and typeset.

PLEASE CITE THIS ARTICLE AS DOI: 10.1063/1.50086370



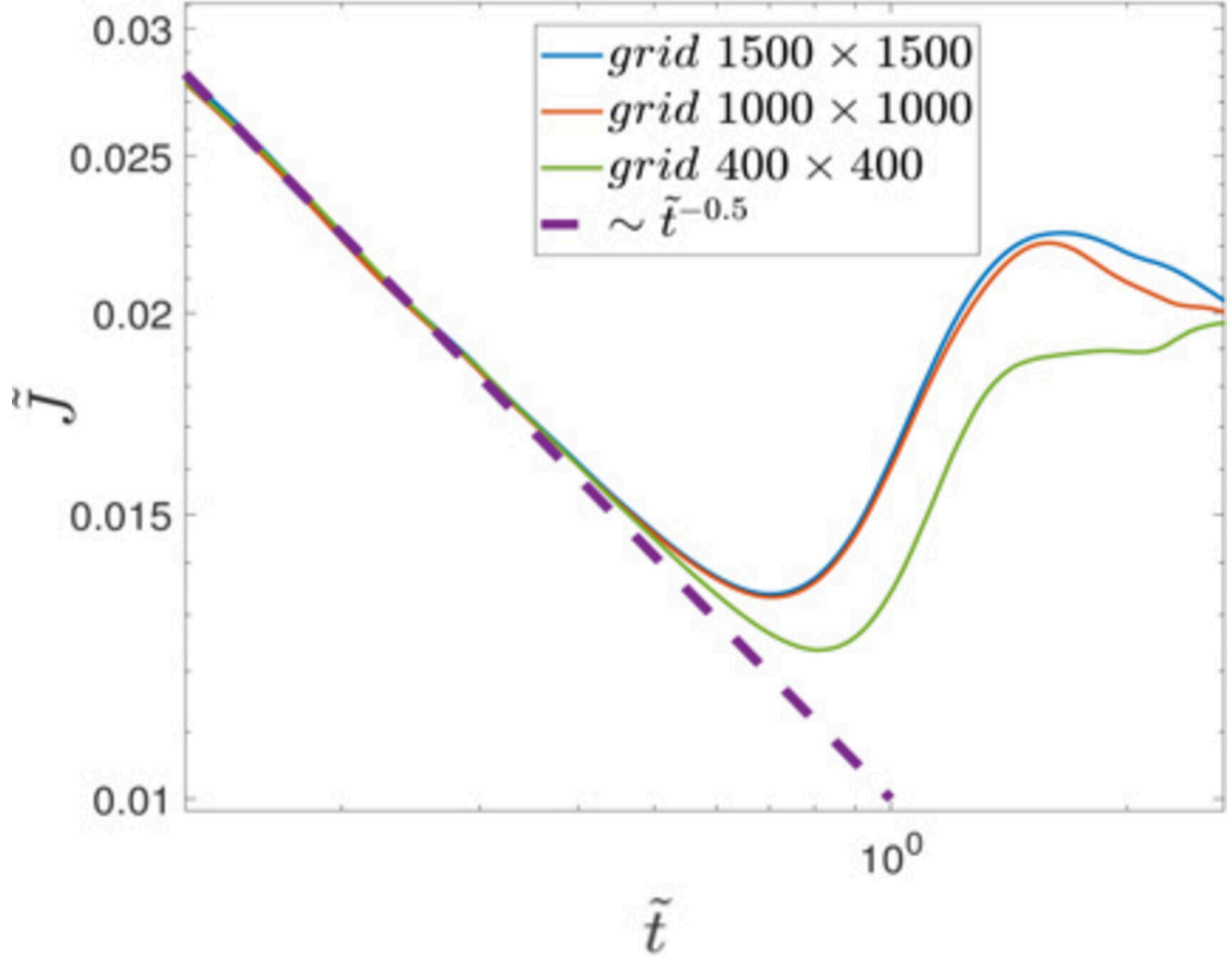
This is the author's peer reviewed, accepted manuscript. However, the online version of record will be different from this version once it has been copyedited and typeset.

PLEASE CITE THIS ARTICLE AS DOI: 10.1063/5.0086370



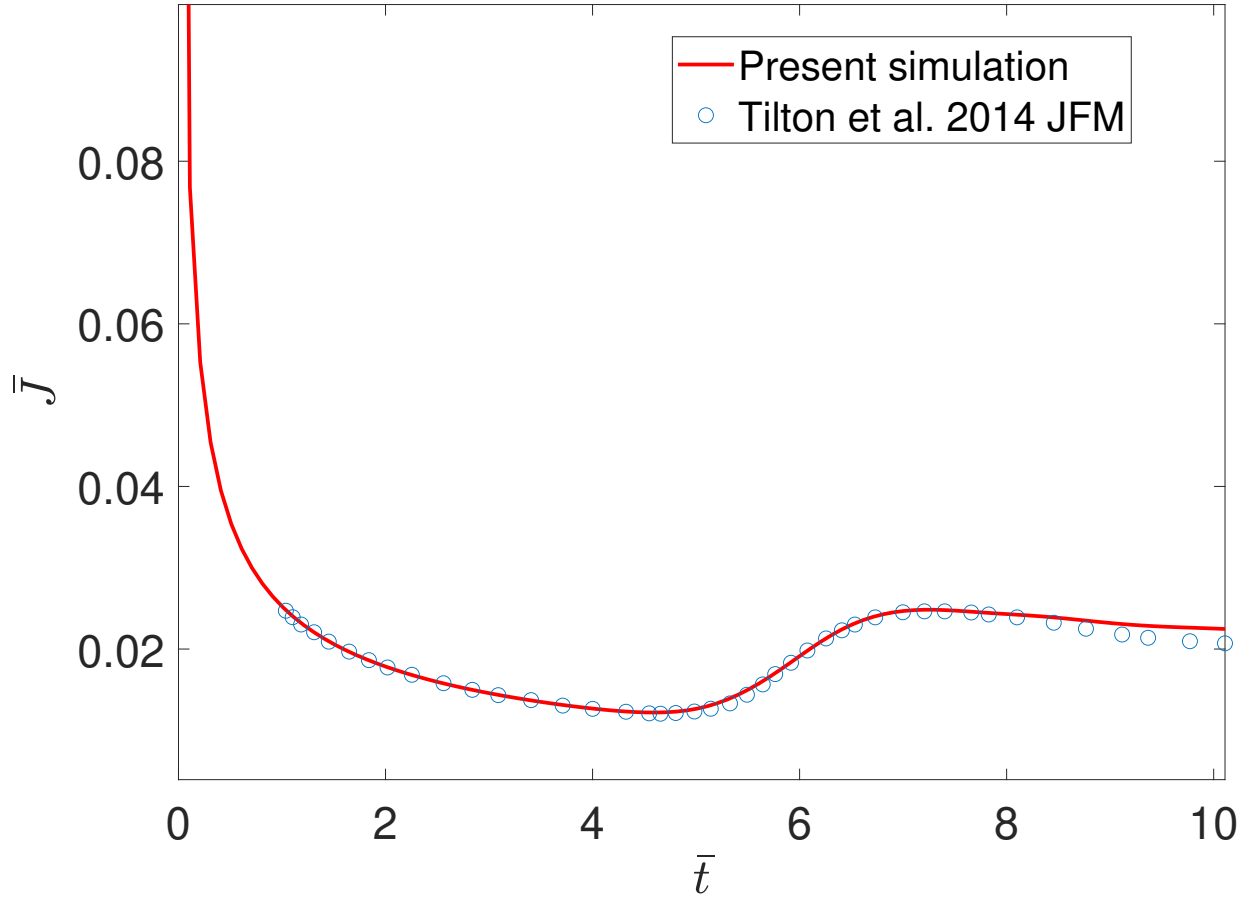
This is the author's peer reviewed, accepted manuscript. However, the online version of record will be different from this version once it has been copyedited and typeset.

PLEASE CITE THIS ARTICLE AS DOI: 10.1063/1.50086370



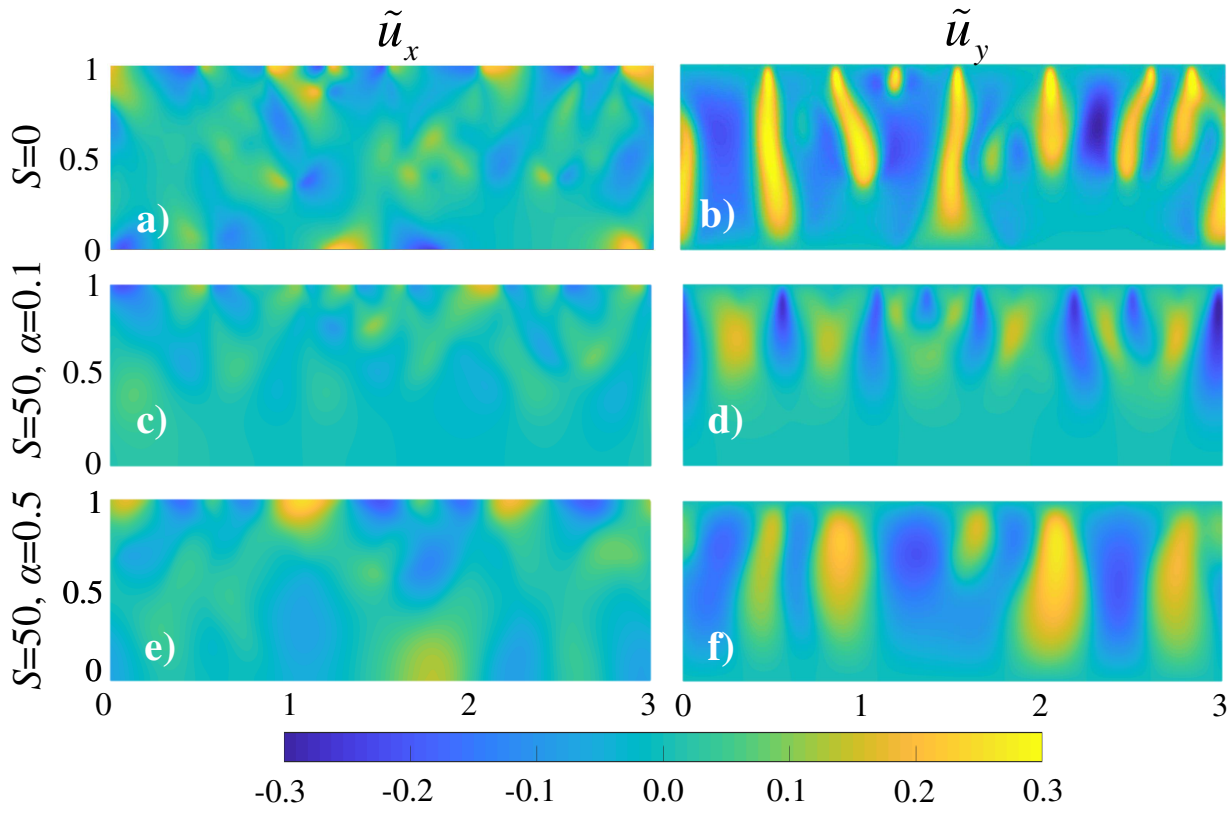
This is the author's peer reviewed, accepted manuscript. However, the online version of record will be different from this version once it has been copyedited and typeset.

PLEASE CITE THIS ARTICLE AS DOI: 10.1063/1.50086370



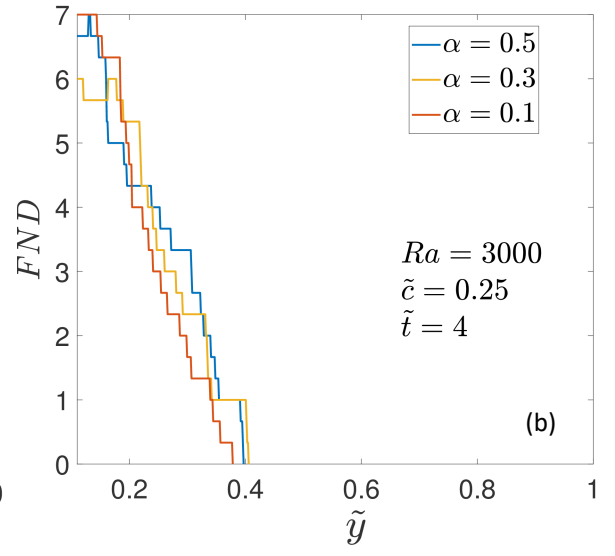
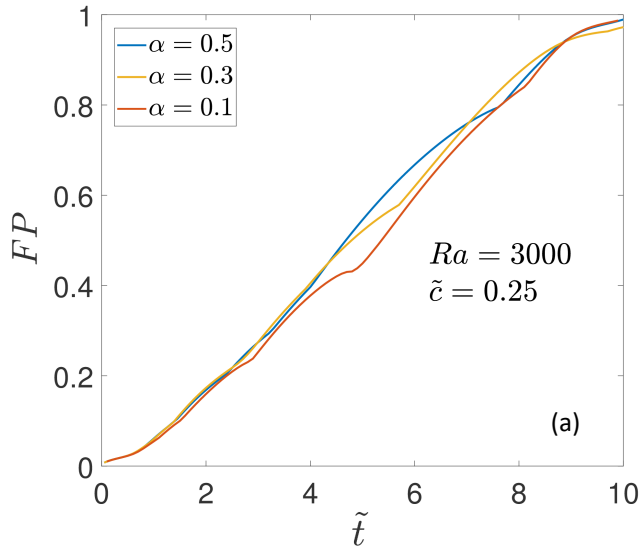
This is the author's peer reviewed, accepted manuscript. However, the online version of record will be different from this version once it has been copyedited and typeset.

PLEASE CITE THIS ARTICLE AS DOI: 10.1063/5.0086370



This is the author's peer reviewed, accepted manuscript. However, the online version of record will be different from this version once it has been copyedited and typeset.

PLEASE CITE THIS ARTICLE AS DOI: 10.1063/1.50086370



This is the author's peer reviewed, accepted manuscript. However, the online version of record will be different from this version once it has been copyedited and typeset.

PLEASE CITE THIS ARTICLE AS DOI: 10.1063/1.50086370

